Optimal Anti-Idling Systems for Service Vehicles

by

Milad Khazraee

A thesis
presented to the University of Waterloo
in fulfillment of the
thesis requirement for the degree of
Doctor of Philosophy
in
Mechanical Engineering

Waterloo, Ontario, Canada, 2016

AUTHOR'S DECLARATION

I hereby declare that I am the sole author of this thesis. This is a true copy of the thesis, including any required final revisions, as accepted by my examiners.

I understand that my thesis may be made electronically available to the public.

Milad Khazraee

Abstract

Vehicles are major sources of air pollution and greenhouse gas emissions, so any improvement in their fuel efficiency can have a significant impact on the environment and economy. In this study, a regenerative auxiliary power system (RAPS) is proposed to prevent engine idling in service vehicles. Besides preventing idling, the proposed RAPS reduces vehicle total fuel consumption by utilizing regenerative braking and an optimal charging strategy. This system employs waste energy during braking and provides the demanded auxiliary power for a service vehicle to prevent idling. In addition, the system can be retrofit onto existing vehicles. In addition, necessary tools, algorithms and methods to arrive at an optimum RAPS for anti-idling of service vehicles are designed, developed, and implemented.

A generic, modular, and flexible vehicle model is created using scalable powertrain components. This model is used by the optimizer to simulate the energy efficiency of the vehicle system in order to minimize the total cost of the system during its expected life cycle. Multi-disciplinary design optimization is applied to optimize the system's component sizes and power management control logic with respect to a cost-based objective function. Two different optimization methods, Genetic Algorithms (GA) and Simulating Annealing (SA), are utilized to find the optimal solution. Different limitations and constraints of utilizing the Electrical Storage Systems (ESS) are considered in the optimization for more accurate results. Expected changes in power consumption and fuel efficiency in the service vehicle equipped with RAPS is presented as a case study. It is shown that utilizing the RAPS has a significant impact on the total fuel consumption of the vehicle.

Based on the results from case study, a prototype model of RAPS (containing generator, battery, auxiliary load, and control system) is developed for laboratory evaluation. Using the RAPS prototype as a hardware-in-the-loop (HIL) of a service vehicle, the proposed system performance is evaluated and the model is validated. It is shown that there is a close match between the experimental and simulation results. The results show that the RAPS is capable to eliminate the idling in service vehicles with considerable fuel saving.

Acknowledgements

I would like to express my deep gratitude to my supervisor, Prof. Amir Khajepour for all of the guidance, support, patience, kindness and constant encouragement during my research. Working with you has been a true privilege and tremendously fortunate.

I would also like to thank my thesis committee, Prof. Roydon Fraser, Prof. Soo Jeon, Prof. Magdy Salama, and Prof. Narayan Kar for their insightful comments and encouragement. Their critiques have helped to improve the quality of my thesis.

My sincere thanks to my colleague Yanjun Huang for all of his support and care. Kevin Cochran and Jeff Graansma in the Mechatronic Vehicle Systems laboratory for their technical help and support. My friends Saeid Khosravani, Brian Fan, Alireza Kasaiezadeh, Yahya Mahmoodkhani and all of my officemates who made a friendly atmosphere during my course of studies at the University of Waterloo.

No word describes my heartfelt thanks to my parents and my brother whose support has always been encouraging throughout my life. This accomplishment would not have been possible without them.

Table of Contents

AUTHOR'S DECLARATION ii
Abstract iii
Acknowledgements v
List of Figures viii
List of Tables ix
List of Abbreviations x
Nomenclature xii
Chapter 1 Introduction 17
1.1 Objectives and Scope of this Research 17
Chapter 2 Literature Review 21
2.1 Anti-idling Technologies in Service Vehicles 21
2.1.1 Stationary Anti-idling Technologies 22
2.1.2 Mobile Anti-idling Technologies 23
2.1.3 Discussion 25
2.2 Multi-disciplinary Design Optimization (MDO) 27
2.2.1 Design Optimization in Hybrid and Electric Vehicles 28
2.3 Summary 29
Chapter 3 Modeling and Configuration 31
3.1 System Configuration and Potential Energy Recovery 32
3.2 System Integration to Powertrain 33
3.2.1 Low Power Demand System (Serpentine Belt) Configuration 34
3.2.1 High Power Demand System (Power Take-Off) Configurations 35
3.3 Components Modeling 41
3.3.1 General Vehicle Model 44
3.3.2 Final Drive (Differential) 45
3.3.3 PTO 45
3.3.4 Transmission (Gearbox) 48
3.3.5 Generator 48
3.3.6 Engine 51
3.3.7 Electrical Energy Storage Systems (Batteries) 55
Chapter 4 Multi-disciplinary Design Optimization and Case Studies 65
4.1 Introduction 65
4.2 Optimization Process Review 65
4.2.1 Optimization Algorithm Structure 66
4.3 Objective Cost Function 69
4.3.1 Fuel Costs 70
4.3.2 Plug-in Electricity Cost 71
4.3.3 Initial RAPS Components' Costs 73
4.3.4 Total Objective Function 73
4.3.5 Limitations and Constraints 76
4.4 Case Studies 79
4.4.1 Case Study: GMC Savana 2500 82

Chapter 5 Experimental Validation 89
5.1 Experimental Setup: Hardware-In-the-Loop (HIL) 89
5.2 Experiments Procedure 96
5.2.1 Alternator-Generator Characterization Experiments Procedure 96
5.2.2 RAPS Total Model Validation Experiment Procedure 99
Chapter 6 Concluding Remarks and Future Work 103
6.1 Thesis Contributions 104
6.2 Future Work 106
6.2.1 Modifying the Optimization Process 106
6.2.2 Considering Service Vehicle Cargo Weight Cost 107
6.2.3 Different EES and Battery Pack Degradation Function 107
6.2.4 Field Testing Prototype 108
Bibliography 109
Appendix A Optimization Methods 114

List of Figures

Figure 2-1: Truck stop electrification (TSE) station: an example of off-board stationary anti-idling technologies [16]. 23
Figure 2-2: Solar energy powered auxiliary service vehicles [17] 24
Figure 3-1: Regenerative auxiliary power system (RAPS) configuration 32
Figure 3-2: Available space to install generator in the low power demand targeted vehicle "Ford Transit Connect Cargo XL-2010" 34
Figure 3-3: Low power demand systems (the serpentine belt) configuration 35
Figure 3-4: Possible power extraction (PTO installation) points in the high power demand system configuration 36
Figure 3-5: "Split-Shaft" PTO [40] 37
Figure 3-6:"Side Countershaft" PTO [41] 38
Figure 3-7: "Transmission Aperture" PTO 39
Figure 3-8: General forward-looking vehicle model 42
Figure 3-9: General backward looking vehicle model 43
Figure 3-10: Power management controller input/output signals 47
Figure 3-11: Willan's line modeling concept [43] 52
Figure 3-12: Common electric circuit-based models for batteries [49] 56
Figure 4-1: Optimization software scripts 66
Figure 4-2: Optimization process 68
Figure 4-3: General Drive Cycle 80
Figure 4-4: Industry Partner Drive Cycle 81
Figure 4-5: Service Vehicles Auxiliary Load Suggested by Industry Partner 82
Figure 5-1: Hardware-in-the-loop facilities installed in the Mechatronic Vehicle Systems laboratory 90
Figure 5-2: a) Electrical part of RAPS prototype model; b) Load box (Auxiliary load simulator in low power demand configuration) 92
Figure 5-3: Schematic installation connection for low power demand (serpentine belt) configuration 93
Figure 5-4: Schematic installation connection for high power demand (aperture PTO) configuration 94
Figure 5-5: Conceptual picture of "Mustang Dynamometer" (HIL test stand) [59] 95
Figure 5-6: Alternator connection to the dynamometer 95
Figure 5-7: Systematically increasing loading of alternator during maximum current determination at 3300 rpm 97
Figure 5-8: "Maximum current versus alternator angular velocity" curve 97
Figure 5-9: Alternator "Efficiency map" 99
Figure 5-10: Experiment drive cycle 100
Figure 5-11: Dyno1 (Engine simulator) angular velocity 101
Figure 5-12: Battery SOC changes from RAPS model and RAPS prototype experiment 102

List of Tables

Table 3-1: Chosen battery packs for optimization 62
Table 4-1: Estimated Prices for Added Initial Parts 73
Table 4-2: Optimization variables description (related to equation (4-8)) 75
Table 4-3: Assumed output power of different chosen battery models 79
Table 4-4: GMC Savana 2500 Specifications 83
Table 4-5: Optimization results for GMC Savana during general drive cycle 84
Table 4-6: Optimization results for GMC Savana during industry partner drive cycle 85
Table 4-7: Vehicle Models Simulation Results 87

List of Abbreviations

A/C-R	Air Conditioning and Refrigeration
AC	Air Conditioning
APU	Auxiliary Power Units
BPS	Battery powered systems
DOD	Depth Of Discharge
DP	Dual Polarization
ESS	Electrical Storage Systems
FCPS	Fuel cell powered systems
FTP75	Federal Test Procedure
GA	Genetic Algorithms
HEV	Hybrid Electric Vehicle
HIL	Hardware-In-the-Loop
HPPC	Hybrid Pulse Power Characterization
HWFET	HighWay Fuel Economy Test
ICE	Internal Combustion Engine
MDO	Multi-disciplinary Design Optimization
NYCC	New York City Cycle
OBD	On-Board Diagnostics
OEM	Original Equipment Manufacturer
PTO	Power Take-Off
RAPS	Regenerative Auxiliary Power System
SA	Simulating Annealing

SOC	State Of Charge
TES	Thermal Energy Storage
TSE	Truck Stop Electrification
UDDS	Urban Dynamometer Driving Schedule

Nomenclature

A	Frontal area of vehicle
A_{Des}	Longitudinal acceleration of vehicle
a_1	Optimization fuel consumption weighting coefficient
a_2	Optimization plug-in electricity weighting coefficient
a_3	Optimization battery pack weighting coefficient
B	Engine cylinder bore
$B(X_D)$	Total battery pack cost
b_4	Optimization capital cost coefficient
C_1	Long time transient capacitance of battery
C_2	Short time transient capacitance of battery
C_D	Drag coefficient
$C_{Act-PTO}$	Power take off activation control signal
C_{RR}	Rolling resistance of the tire
$C(X_D)$	Optimization constraints vector
E	Optimization error signal coefficient
e	Energy conversion efficiency in the ICE
e_E	Thermodynamic properties of the engine related to the mean effective pressure
F_{Drag}	Total vehicle aerodynamics drag force
F_{Drive}	Vehicle drive force
F_{RR}	Total tire rolling resistance force
F_{Total}	Total vehicle longitudinal force
$F\big(U(X_D)\big)$	Total fuel consumption of the vehicle in five years

$f(U(X_D))$	Total fuel consumption of the vehicle for one active day
g	Gravitational acceleration
H_L	Fuel lower heating value
I_B	Battery current
I_{B_Ideal}	Battery current in the ideal condition
I_G	Generator output current
$J(X_D, U(X_D))$	Optimization objective function
k_1	Experimental parameters
k_2	
k_3	
k_4	
M_{Cargo}	Cargo weight of the vehicle
M_{EES}	Mass of electrical energy storage and other electrical parts
M_{Total}	Total vehicle mass
M_{Veh}	Vehicle mass without electrical energy storage or cargo
$\dot{m}_F$	Fuel mass flow
N	Number of engine stroke
N_G	Generator ratio due to serpentine belt pulleys
N_F	Final drive ratio
N_{PTO}	Power take off gear ratio
N_T	Transmission ratio
P_{B_Actual}	Actual change in the battery stored power
P_{B_Desired}	Desired change in the battery stored power
P_{Drive}	Total drive power demand

P_{Fuel}	Enthalpy flow associated with fuel mass flow
P_G	Generator output electrical power
P_{Lost}	Lost power in the powertrain system
$P(U(X_D))$	Total plug-in electricity consumption of system in five years
p_L	Total engine losses
p_{LF}	Engine mean effective pressure losses due to friction
p_{LG}	Engine mean effective pressure losses due to gas exchange
p_{ME}	Engine mean effective pressure
p_{MF}	Fuel available mean effective pressure
$p(U(X_D))$	Total plug-in electrical energy purchased after one active day
R_1	Series resistance of battery
R_2	Long time transient resistance of battery
R_3	Short time transient resistance of battery
S	Engine stroke
T_{DL}	Final drive torque
T_E	Engine total demanded torque
T_{E_Charge}	Engine demand torque for direct battery charging
T_G	Generator torque
T_{PTO-In}	Input torque of power take off
$T_{PTO-Out}$	Output torque of power take off
T_R	Torque required to overcome the engine resistance forces (Engine idling torque)
T_T	Transmission torque
T_{Wheel}	Drive wheels torque
$U(X_D)$	Optimization Simulink model simulation result outputs

V_1	Terminal voltage of battery
V_2	Long time transient voltage of battery
V_3	Short time transient voltage of battery
V_{B_OC}	Battery open circuit voltage
V_{Des}	Longitudinal velocity of vehicle
V_{ED}	Engine displacement (volume)
V_G	Generator output voltage
V_{MP}	Mean piston speed
W_{In}	Available input energy for conversion (Willan's line modeling formula)
W_{Loss}	Total power loss in the energy converter (Willan's line modeling formula)
W_{Out}	Actual useful output energy of the converter (Willan's line modeling formula)
X_D	Optimization design variable candidates vector
α	Road grade angle in radian
α_{Reg}	Regenerative braking coefficient
η	Efficiency of the energy converter (Willan's line modeling formula)
η_E	Engine efficiency
η_F	Final drive efficiency
η_G	Generator drive efficiency
η_{PTO}	Power take off efficiency
η_T	Transmission efficiency
Π_{max}	Maximum engine boost pressure
ρ	Air density
ω_{DL}	Final drive angular velocity
ω_E	Engine demanded angular velocity

ω_G	Generator angular velocity
ω_{PTO-In}	Input angular velocity of power take off
$\omega_{PTO-Out}$	Output angular velocity of power take off
ω_T	Transmission angular velocity
ω_{Wheel}	Drive wheels angular velocity

Chapter 1

Introduction

The daily work cycle of service vehicles consists of many loading and unloading stops. During these stops, their auxiliary devices such as Air Conditioning (AC) and refrigeration units that are powered by the engine need to be active in order to hold the storage conditions required for their parcels. In such situations, the engine runs at its idling speed resulting in extremely low fuel efficiency. Idling fuel efficiency is estimated to be between 1% and 11%; whereas, at highway speeds diesel engines could provide up to 40% efficiency [1]. In addition, engine wear and greenhouse gas emissions increase remarkably during idling. These drawbacks of vehicular idling justify governmental regulations enacted in many countries against idling. The proposed solution in this study is to address the need for anti-idling systems in service vehicles.

1.1 Objectives and Scope of this Research

In this thesis, regenerative auxiliary power systems (RAPS) are proposed as a solution for anti-idling systems. As will be reported in the literature review chapter, there is an increasing attempt and demand for anti-idling systems. The target of any anti-idling system is to decrease the main drawbacks of idling – low fuel efficiency, high emissions, and engine wear. The reported idle-reduction methods in the literature try to manage the fuel consumption or send the fuel directly to the auxiliary device. With the exception of the full hybrid method, none of the other idle-reduction methods utilize the waste energy.

The proposed RAPS method employs the waste energy during braking and provides the demanded auxiliary power for service vehicles. This solution will decrease the fuel consumption without a high increase in the total system weight and initial cost due to its minimal modification in the existing system. In order to improve the efficiencies of the power extraction system and decrease fuel consumption, a RAPS charges the batteries from the wasted kinetic energy of the vehicle during braking. The proposed system has the following benefits:

i) Maximizes the use of regenerative braking energy;

ii) Improves the fuel efficiency;

iii) Minimizes the system costs over the life of the RAPS;

iv) Satisfies the auxiliary power demand of a service vehicle;

v) Minimizes the modifications to the existing vehicle drivetrain in order to make the design acceptable and affordable for the industry.

If regenerative braking energy is not sufficient to charge the batteries, the power management controller charges the batteries directly from the engine during peak engine performance. In addition, the system allows for plug-in charging to reduce running costs even further.

Fleet companies use different service vehicles with various power requirements for their auxiliary devices. Hence, one RAPS design will not fit all. This study is intended to design, develop, and implement the necessary tools and methods to arrive at an optimum RAPS for a given service fleet. Generally, the proposed RAPS includes an ESS, transmission, and power electronics. All of these should be optimized for cost, performance, and simplicity based on the power requirements of the targeted service vehicle.

Since there are different parts with different disciplines in the RAPS, a Multi-disciplinary Design Optimization (MDO) technique is used to optimize the overall system configuration, size of components, and power management. The optimizer objective function will be defined from the cost perspective, where the objective is to minimize the total cost of the system through balancing the size of the Electrical Energy Storage (EES) devices and optimize the power management control while minimizing the Internal Combustion Engine (ICE) fuel consumption. The models are evaluated using Hardware in the Loop (HIL) experimental data.

1.2 Thesis Outline

The modeling and optimization process of this research are explained in the first part of this thesis followed by the model verification experiments and results of case studies. Chapter 1 provides a brief description of the need for a better energy management solution in service vehicles and presents the proposed solution in this study. The objectives of this work and the general steps towards fulfilling these objectives are also provided.

The literature review and background regarding service vehicles along with the anti-idling technologies in the literature and industry are presented in Chapter 2. Furthermore, the idea of multi-disciplinary design optimization and examples of this concept's application to electric and hybrid vehicles are briefly reviewed.

Possible configurations of the RAPS are discussed in Chapter 3. Moreover, different options for the integration of RAPS with vehicle powertrains and the limitations of each configuration are explained. The details of the components' modeling and the utilized backward modeling concepts are demonstrated.

In Chapter 4, the focus is on the MDO. The background information on common optimization methods in hybrid vehicles is briefly reviewed, and the optimization process and developed algorithmstructure in this study are explained. Furthermore, different cost functions of the total optimizer objective function are described and the specifications of the chosen batteries for the optimization and simulation are presented. In the second part of this chapter, the expected impacts of utilizing the proposed system on fuel consumption in service vehicles are presented as case study.

Experimental verification and Hardware in the Loop (HIL) test stand are discussed in Chapter 5. In this chapter, laboratory evaluations utilizing testbed are used in order to verify the modeling and optimization results in the prototype RAPS. The experimental procedures are briefly explained and the tests results are shown.

A summary of the research and possible future works for this study are provided in Chapter 6.

Chapter 2

Literature Review

This chapter reviews the related background information for this study. Different anti-idling (or idle reduction) technologies used in service vehicles are explained, and the benefits and limitations of the different types are compared. In the second part of this chapter, MDO is briefly discussed and different examples of design optimization in hybrid and electric vehicles are mentioned.

2.1 Anti-idling Technologies in Service Vehicles

Service vehicles that are equipped with Air Conditioning and Refrigeration (A/C-R) devices are categorized as A/C-R service vehicles. These groups of vehicles are mostly used by fleet companies to move and deliver different products. A/C-R service vehicles include a wide range of vehicles from cargo and minivans to refrigerators and box trucks. In most cases, these vehicles are equipped with auxiliary devices to provide the necessary storage conditions for the products or comfort conditions for the passengers they carry. Service vehicles have many loading and unloading stops during their work cycle. At these stops, their auxiliary devices, such as AC and refrigeration units, should be active, and the engine should work during these idling periods to power the auxiliary devices.

During idling time, the engine works at very low efficiency conditions, 1 to 11 percent for diesel engines. Considering the fact that for A/C-R service vehicles, 15 to 25 percent of engine fuel consumption goes to auxiliary devices [2], [3], utilizing an anti-idling solution is necessary.

Besides low engine efficiency and high fuel costs, idling increases greenhouse gas emissions, the level of noise pollution, and engine wear. The impact of idling on the environment, economy, and human health forces the governments to establish new regulations [4], [5]. Different anti-idling or idle-reduction technologies have been utilized as mentioned in [6]–[15]. Generally, all of these technologies can be classified in two main groups: mobile and stationary.

2.1.1 Stationary Anti-idling Technologies

This type of anti-idling technology can be used when the vehicle is stationary. Moreover, special stations should be constructed in the working area of service vehicles. These stations and service vehicles should be equipped with devices to let service vehicles purchase services such as heating, cooling, and electricity. This type of anti-idling technology is known as a truck stop electrification (TSE) system. If the purchased services are provided through an external device, as shown in Figure 2-1, the system is considered as an off-board system. If the service is purchased as electricity and there is a need for installation of heating and cooling systems and electrical converters in the service vehicle, the system considered an onboard system. The examples of these technologies are the industrial products of Shorepower Technology, CabAire LLC, IdleAire, Envirodock and AireDock.

Figure 2-1: Truck stop electrification (TSE) station: an example of off-board stationary anti-idling technologies [16]**.**

2.1.2 Mobile Anti-idling Technologies

In order to use mobile anti-idling systems, extra devices should be installed in service vehicles. There are different types of mobile anti-idling technologies that can be arranged in the following groups:

- **Auxiliary Power Units (APUs)**

In these systems, a small ICE is added to the service vehicle. Auxiliary devices, especially compressors, can be directly connected to the output of this engine. In another configuration, all-electric auxiliary devices are powered by a generator which is directly connected to a small ICE. In each of these configurations, the small ICE consumes fuel from the truck's fuel tank. Examples of these technologies are the industrial products of Pony pack, Thermo King's TriPac, Willis-branded, Dometic, Rigmasterpower and Dynasys.

- **Automatic Engine Shutdown devices**

In these systems, an engine management system is added to the service vehicle. Using this system, the operator programs the vehicle's engine to turn on and off based on parameters

such as the preset period of time, engine temperature or efficiency condition, and battery voltage.

- **Electrical Storage Systems (ESS) powered**

In these types of anti-idling systems, the required power of the auxiliary devices is provided by the ESS. Generally, there are three types of ESS powered anti-idling systems: **i) Battery powered systems (BPS):** This ESS is a bank of batteries that are recharged by the service vehicle's engine during vehicle operation or by plug-in electricity during stop periods. **ii) Fuel cell powered systems (FCPS):** This ESS is a fuel cell pack. **iii) Solar energy systems**: This ESS is a bank of batteries which are recharged by the electrical energy from solar cells as shown in Figure 2-2.

Figure 2-2: Solar energy powered auxiliary service vehicles [17]

- **Direct-fired heaters**

This anti-idling technology is considered as a partially functional anti-idling device since it cannot perform all the responsibilities of all auxiliary devices. Utilizing direct-fired heaters,

fuel is imported from the fuel tank and burned in a small assembly to provide cabin space heating.

- **Thermal Energy Storage (TES)**

In systems utilizing TES, thermal energy (heat/cold) is stored as a change in the internal energy of the storage's material during the active time of the vehicle. This energy can later be used while the vehicle is turned off [18], [19].

- **Hybrid Diesel Trucks**

Electric or hydraulic hybrid power systems are utilized in service vehicles to decrease their total fuel consumption. In these systems, an extra motor is added to the system to handle parts of the main engine's responsibilities using the stored electrical or hydraulic energy. Examples of these technologies include the industrial products of Eaton, Freightliner, GM, Mercedes Benz, Mitsubishi Fuso Truck & Bus Corporation, Hino Motors, and UD Trucks.

2.1.3 Discussion

Stationary anti-idling technologies are not a suitable solution for service vehicles with frequent stops, and especially unsuitable for city service vehicles. These vehicles mostly distribute food products through a city; as such, if stationary technologies are used, most supermarkets receiving food via these service vehicles would require a station. This financially unfeasible since service vehicles have multiple deliveries a day. Service vehicles cannot charge their batteries completely during these stops, and not all supermarkets would be able to afford the required station devices.

Among the mobile anti-idling technologies, APUs and direct-fired heaters are the most conventional and popular anti-idling solutions. Direct-fired heaters are partially functional anti-idling devices and do not have any benefit to A/C-R devices. APUs usually provide all the demanded auxiliary power. However, an added engine and generator will increase the weight and noise level of the vehicle. In addition, considering the installation and maintenance expenses, the total system and fuel costs may not decrease remarkably since the major advantage of these systems is in their use of a small engine to prevent the main engine's low-efficiency auxiliary support.

Automatic engine shutdown devices are easy to install, have lower costs, and reduce idling time; however, they do not have any benefits in powering auxiliary devices. ESS anti-idling technologies are considered as the main alternative for conventional APUs. The added engine and generator in APUs are replaced by ESS packages, especially batteries. This will eliminate extra emissions and noise associated with APUs. However, their disadvantages include a higher cost and weight.

In BPS, a generator powered by the engine recharges the batteries. In such systems, the batteries can be charged when the engine operates at higher efficiency. Fuel cell powered systems and solar energy systems are expensive and not yet fully commercialized [14] for anti-idling applications.

As the commonly used anti-idling technologies such as APUs and BPS do not use any regenerative power, in this project, an optimal Regenerative Auxiliary Power System (RAPS) is proposed to improve the efficiency and reduce costs. The proposed system provides the

demanded auxiliary power for an A/C-R service vehicle using regenerative energy and the engine when needed.

In summary, the proposed RAPS is an optimized solution to maximize fuel economy while minimizing costs over a given life of the RAPS. Modeling, component sizing, optimization, and optimal power management are the steps taken in the remainder of this thesis to achieve the development of the proposed anti-idling system.

2.2 Multi-disciplinary Design Optimization (MDO)

Complex engineering systems consist of different components, which use various disciplines and concepts to work. Dealing with these engineering systems and performing design and optimization requires various engineering knowledge, and in most cases, a group of engineering teams with different specializations and disciplines work together to find the desired solution with acceptable conditions.

MDO is a field of engineering that utilizes optimization methods to solve design problems in those complex systems with a variety of disciplines. Using MDO, engineers can unify all required disciplines simultaneously and increase the efficiency of the design process. These problems could become very complicated given their multi-disciplinary nature. MDO has been used in different engineering systems, for instance, in underwater autonomous vehicles [20], spacecraft launch vehicles [21] and different aerospace design optimization [22], vehicle suspension and dynamics [23]–[25], automotive design [26], [27], linkage mechanism design [28], and rocket design [29].

2.2.1 Design Optimization in Hybrid and Electric Vehicles

In the area of hybrid and electric vehicles, different MDO have been applied primarily in two areas: i) component and powertrain sizing, ii) power management logic and control strategy. There are also studies that consider both optimizations simultaneously.

Simulated annealing and genetic algorithms are utilized by Gao *et al.* [30] to optimize a parallel hybrid electric vehicle (HEV) powertrain to increase the overall fuel economy. The vehicle is modeled in PSAT software [31] against a composite city and highway driving cycle. ADVISOR [32] is the other common vehicle modeling software that is utilized in the works of Zhang *et al.* [33], Fang *et al.* [34], and Liu *et al.* [35]. A genetic algorithm is used to improve the fuel economy and reduce vehicle emissions for a series hybrid electric vehicle by Zhang *et al.* [33]. Both powertrain sizing and the power management logic are considered for optimization against one highway (HWFET) drive cycle and one city (UDDS) drive cycle. In the work of Fang *et al.* [34], the powertrain sizing and control system of a parallel hybrid electric vehicle are considered for optimization. The purpose of this optimization is to minimize fuel consumption and reduce emissions (CO, HC, and NO_x) using a genetic algorithm. Liu *et al.* [35] consider a series hybrid electric mini-bus and utilize a genetic algorithm. The optimization goal is to minimize the fuel consumption of the vehicle based on the desired city-highway drive cycle. In this study, the option of changing the conventional vehicle powertrain is also considered. As a result, it is suggested that the size of the generator and engine increase while the number of battery packs and the size of the electric motor decrease.

Fan *et al.* [36], [37] optimized power management logic and powertrain sizing based on a simplified vehicle model developed in Simulink. Different optimization methods such as the genetic algorithm, pattern search, and simulated annealing were used to improve the fuel economy and reduce vehicle emissions for a series hybrid electric vehicle.

In other studies, the focus is on utilizing different optimization methods in order to find the best power management control strategy. For example, Huang *et al.* [38] and Wang *et al.*[39] consider the same series hybrid electric vehicle, and utilize different optimization methods to optimize the fuel economy and emission (NOx, CO, and HC). Huang *et al.* [38] utilize the genetic algorithm and consider different conditions: fuel power only, electric power only, fuel power plus electric power, and regenerative braking. The optimization control calculates the best operating point of the engine to charge the battery packs and power the electrical motor. On the other hand, Wang *et al.* [39] utilize simulated annealing to find the best solution.

2.3 Summary

Different anti-idling technologies and their advantages and disadvantages were explained in this chapter. As shown, the current anti-idling systems do not utilize regenerative power for operating auxiliary devices during idling. Utilizing an optimal regenerative auxiliary power system is the proposed solution in this study; this system employs waste energy and engine power if needed in order to operate auxiliary devices during service stops.

Considering the complexity of the system, a multi-disciplinary design optimization process is needed to fulfill the objectives of the optimized RAPS. In the next chapter, the

components of the proposed system are modeled with a mathematical representation of the RAPS and component optimization sizing.

Chapter 3

Modeling and Configuration

Many different factors and criteria should be considered in order to design an acceptable RAPS. To power the service vehicle's auxiliary devices from braking recovered energy, a regenerative braking system should be integrated into the vehicle powertrain. The connection of the RAPS to the vehicle powertrain, total system configuration, safety, weight, and size of components are the most important factors. As the first step, integration of the RAPS to the vehicle powertrain should be investigated in detail. It is vital that connection of the RAPS does not cause any major modification to the existing vehicle; otherwise, the initial cost of the total system and the safety concerns will reduce industry interest.

The other important point is that the designed RAPS must be modular and easy-to-install in order to reduce installation time and costs. In addition, this research is intended for use in any service vehicle with auxiliary devices, so RAPS components and especially their models should be generic, modular, and flexible for the creation of scalable powertrains and RAPS component's models.

Given these considerations, in this study, the RAPS components are designed with the different configurations of different powertrains in mind. By utilizing this method, RAPS components can be designed separately and added to an existing vehicle. In the first part of this chapter, the design configuration of the RAPS is discussed, and the two most possible categories for integration configurations are described. The modeling concepts of different RAPS components are explained in the last part.

3.1 System Configuration and Potential Energy Recovery

As illustrated in Figure 3-1, a RAPS consists of different electrical and mechanical parts. Input mechanical energy will be extracted from the vehicle's powertrain through the "RAPS Connection Point". There are different options for this connection point, and they will be explained in later sections. This extracted mechanical energy is in the form of torque and angular velocity. Based on the specifications and limitations of the generator, there is possibility of changing the range of the input angular velocity to the acceptable range of the generator.

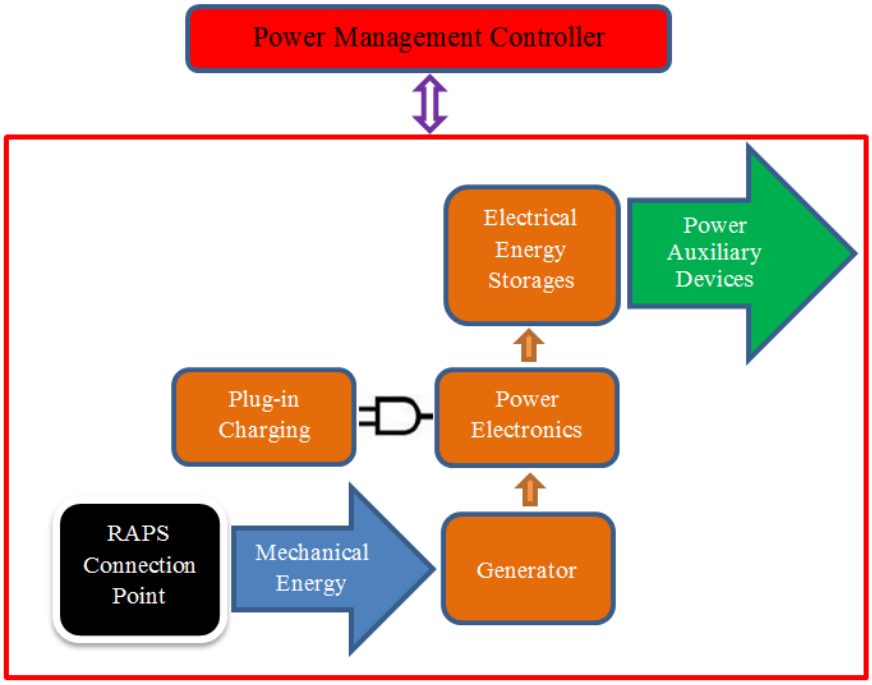

Figure 3-1: Regenerative auxiliary power system (RAPS) configuration

The "Generator" will convert the mechanical energy into electrical energy and produce electrical energy, in the form of current and voltage, to charge the "Electrical Energy Storages". The output energy of the generator will be sent to the "Electrical Energy Storages" through the "Power Electronics" module. The "Power Electronics" module controls the input

energy flow to the “Electrical Energy Storages”. The “Power Electronics” module’s duty is to monitor the electrical energy flow and maintain the current and voltage in a form and range that is suitable for charging the “Electrical Energy Storages”. As previously mentioned, the option for plug-in charging is considered for the proposed RAPS. The “Plug-in Charging” part will send the plug electrical energy to the “Electrical Energy Storages” through the “Power Electronics” module. The “Power Electronics” module has the ability to convert the plug-in AC electricity to the acceptable DC power by the “Electrical Energy Storages”.

The “Electrical Energy Storages” stores the electrical energy and provides power to the vehicle’s auxiliary devices. The “Power Management Controller” will monitor the power demand, battery state of charge (SOC), vehicle status, and brake pedal signal, and based on these conditions, it will control the system’s power flow. It should be noted that the one-way arrows in Figure 3-1 show the power flow in the RAPS, but the two-way arrow between the whole RAPS and the “Power Management Controller” is the flow of data and state conditions information.

3.2 System Integration to Powertrain

There are different parts in a vehicle powertrain that can be used to extract mechanical power for the generator. Possible configurations can be categories in two main groups based on the amount of the demanded power; however, as explained in detail in the following sections, the limitation of the powertrain and connecting components are also very important in this classification. The two main groups of possible configurations are defined as:

3.2.1 Low Power Demand System (Serpentine Belt) Configuration

For service vehicles with low power demands, it can be considered that the generator, which is mostly an alternator in this configuration, is connected to the engine's serpentine belt. The serpentine belt is a continuous belt used to power different devices, which are extracting their power directly from the engine. In this system, the serpentine belt connects the engine crankshaft to multiple devices including the alternator, water pump, air pump, air conditioning compressor, power steering pump, etc. In service vehicles, there is usually a space allocated to the attachment of another device, usually a compressor, to be powered by the serpentine belt. In the design of RAPS with low power demands, this space, as shown in Figure 3-2, can be used to install the extra generator. In addition, for service vehicles without this extra space, there is the option to utilize a higher output alternator instead of the Original Equipment Manufacturer (OEM) alternator.

Figure 3-2: Available space to install generator in the low power demand targeted vehicle "Ford Transit Connect Cargo XL-2010"

Figure 3-3 shows schematically the low power configuration and attachment of the generator to the engine. In this figure, the small arrows show the mechanical or electrical power flow and the big arrows emphasizes the direction of the energy flow. The drawback of the low power demand configuration is that the maximum captured kinetic energy during braking is limited by the size of the generator-alternator. Thus, the regenerative energy is limited by the available space for the generator and the characteristics of the serpentine belt, especially its maximum tension capacity. This configuration is the main solution for vehicles, such as front wheel drive vehicles, with little space for adding the generator to the powertrain.

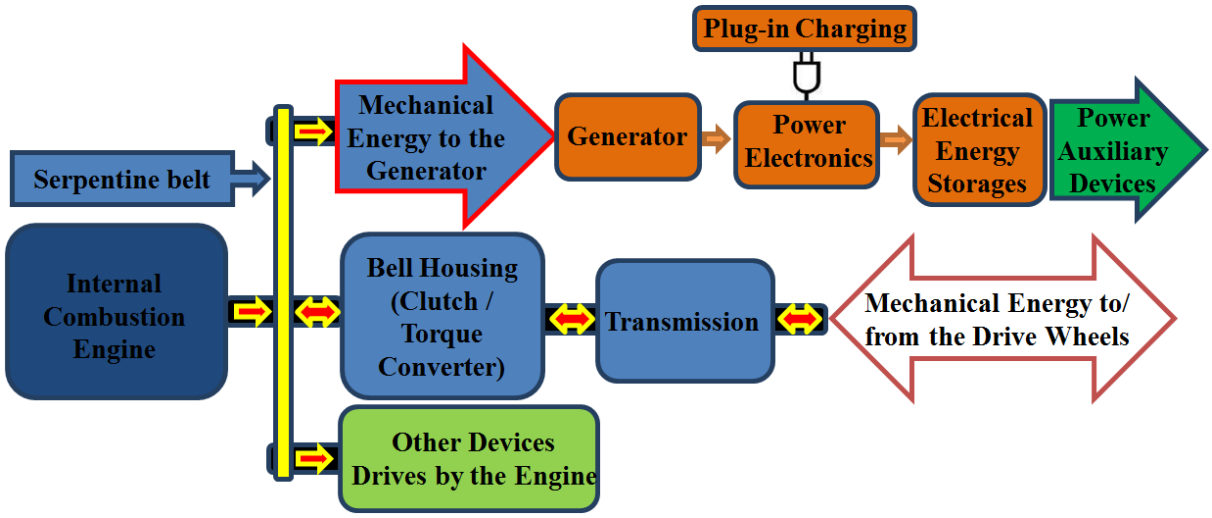

Figure 3-3: Low power demand systems (the serpentine belt) configuration

3.2.1 High Power Demand System (Power Take-Off) Configurations

In service vehicles with high power demands, the generator can be driven by a power take-off (PTO) module. In a vehicle, the engine produces power and transfers it to the wheels through the bell housing, transmission, drive shaft, differential and final axles. This condition can be better illustrated in a rear drive vehicle schematic as shown in Figure 3-4. In theory, it

is possible to extract the mechanical power for the generator from 6 locations. However, PTO should allow RAPS to run directly from the engine when the vehicle is stopped. This option is possible if a PTO can be installed at a point between the engine and the transmission.

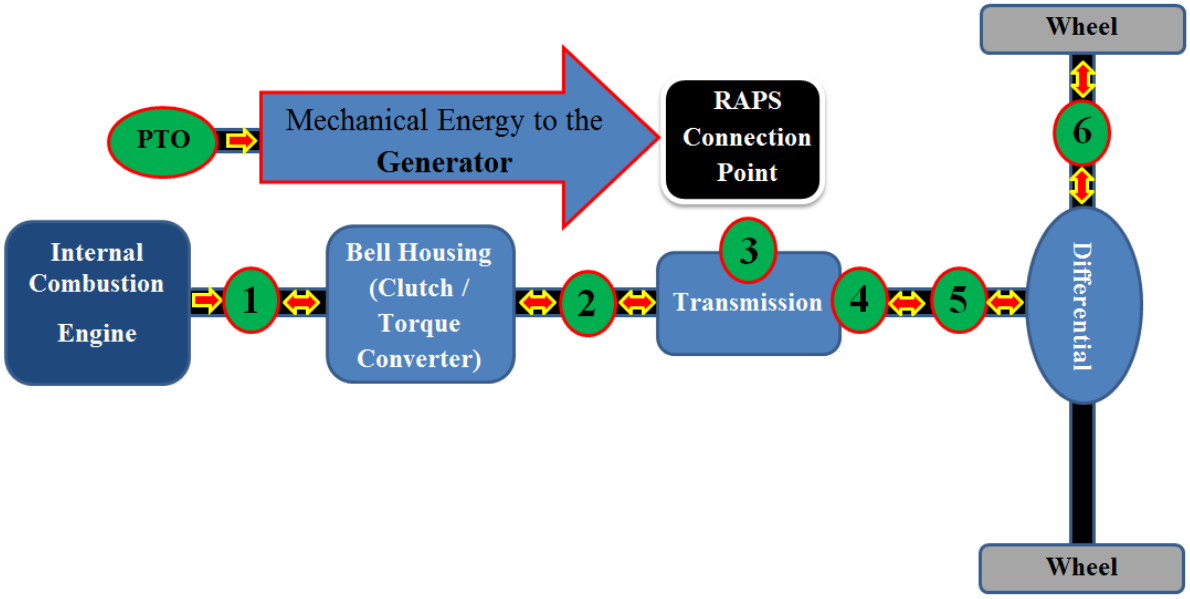

Figure 3-4: Possible power extraction (PTO installation) points in the high power demand system configuration

In order to extract power at each of these points, a different PTO is needed. Generally, the required PTOs can be categorized into three main types:

- "Split-Shaft" PTO: As shown in Figure 3-5, there are different designs and sizes for this kind of PTO. In split-shaft PTOs, the input shaft runs two output shafts where one is a through shaft and the other is for power take off. Considering Figure 3-4, this type of PTO can be used in the following points:

  Point 1: Shaft connecting engine to the bell housing

  Point 2: Connecting the shaft of the bell housing and the transmission

  Point 5: Driveline shaft (drive shaft)

Point 6: Any of the axles

Figure 3-5: "Split-Shaft" PTO [40]

It should be considered that in order to install the split-shaft PTO, one of the power transferring shafts of the existing vehicle requires modification; also, for any of the considered points there should be enough space to install the PTO. Hence, from all the possible installation points for a split-shaft PTO, Point 5 is the most acceptable one. This location, however, does not allow the generator to run directly from the engine when the vehicle is stationary. Some split-shaft PTOs have a clutch, which disconnects the through shaft from the input. This type of PTO could be an option; however, it requires driver action which may make this solution generally undesirable.

- "Side Countershaft" PTO: These types of PTOs are most common, and normally, they are just referred to as PTO – without any prefix. As shown in Figure 3-6, these

PTOs will be installed to the output of the transmission. In most service vehicles or heavy-duty vehicles there is a place to install these PTOs. Considering Figure 3-4, this type of PTO can be used in:

Point 4: Transmission output to the drive shaft

However, installing a PTO for generator power extraction at Point 4 has the same setback as Point 5 and may not be desirable.

Figure 3-6:"Side Countershaft" PTO [41]

- "Transmission Aperture" PTO: In most heavy-duty vehicles, especially service vehicles, the option for mechanical powering of extra devices has been allocated. In these cases, as shown in Figure 3-7, the vehicle transmission has a special place for installing a "Transmission Aperture" PTO to power up other devices. Considering Figure 3-4, this type of PTO can be used in :

  Point 3: Transmission aperture

Figure 3-7: "Transmission Aperture" PTO

There are different scenarios that should be considered for all configurations:

I) Braking: It is expected that RAPS employs the waste energy during braking and maximizes the use of regenerative braking energy. The system will be considered to be in the regenerative braking phase if all the following conditions are true:

1. The vehicle is braking (braking signal is sent to the controller)
2. The vehicle speed is higher than a threshold (higher than 16 Km/h based on suggestion by [42])
3. The EES is not full (battery SOC level is lower than 100%)

For a low power demand system (serpentine belt) configuration during braking, in an automatic transmission, the torque converter still gets braking powers from the drive wheels to pass on to the serpentine belt. However, in manual transmissions (or automatic transmissions at very low vehicle speeds) during braking, the clutch will disconnect the engine-belt from the transmission (or the torque converter does not pass the remaining

braking energy); thus, regenerative braking energy is just part of the kinetic energy in the crankshaft and moving inertia of the engine.

For the high power demand system (PTO) configuration, segments of the drive wheel braking powers, kinetic energy in the crankshaft, and moving inertia of engine during braking can be converted into the regenerative braking power. For this configuration, in manual transmissions during braking, the clutch will disconnect the engine from the transmission and other parts of the driveline. Therefore, if point 1 is considered as the RAPS connection point to vehicle drivetrain, regenerative braking energy will be just part of the kinetic energy in the crankshaft and moving inertia of the engine. Conversely, if any of points 3, 4, 5, and 6 is considered as the connection point, regenerative braking energy will be limited to part of the braking power from the drive wheels. It should be noted that in most vehicles targeted for high power demand configuration, the bell housing (clutch / torque-convertor) is a part of transmission package since connection point 2 will have the same conditions as connection point 3 in most cases.

For the high power demand system (PTO) configuration in automatic transmissions, the bell housing will not disconnect any part of the vehicle powertrain during braking; thus, regenerative braking energy can be obtained from the drive wheel braking powers, kinetic energy in the crankshaft, and moving inertia of engine altogether. Additionally during very low vehicle speeds, the second condition of the regenerative braking phase is not satisfied; therefore, there will be no regenerative braking when that bell housing disconnects the engine from the other parts of vehicle powertrain.

II) Vehicle movement: If regenerative braking energy is not sufficient to charge the batteries, the power management controller charges the batteries directly from the engine during peak engine performance. In this scenario, since the moving power is transferred from the engine all the way to the drive wheels, RAPS can extract the power in all of the aforementioned possible configurations.

III) Vehicle stops: The RAPS target is to prevent the vehicle from idling; hence, while the vehicle is stopped, the engine ought not be active. During long stops, the auxiliary devices' power consumption decreases the battery SOC to a critical level. In this condition, the system should allow a generator to be run directly from the engine when the vehicle is stopped. A serpentine belt configuration will work without any limitations in this scenario. For the PTO configurations, the power extraction point should be anywhere between the engine and the vehicle transmission, or the option of a PTO with a disconnecting clutch and driver action should be considered.

Given all of these scenarios, the "Transmission Aperture" PTO is the ideal and most cost effective solution for the realization of the RAPS in high power demand service vehicles.

3.3 Components Modeling

As the system model will be used for the optimization process, the components' models should be generic, modular, and flexible. The components' models need to be scalable so that the optimization method can determine their optimal sizes.

There are two modeling approaches that can be used:

a) **Forward-looking:** As shown in Figure 3-8, modeling and simulation starts from the driver's point of view. The driver's demanded power is sent to the powertrain

components, and the resulting power that is available from the powertrain is fed to the final drive and wheels. This type of modeling is more realistic compared to the backward looking models.

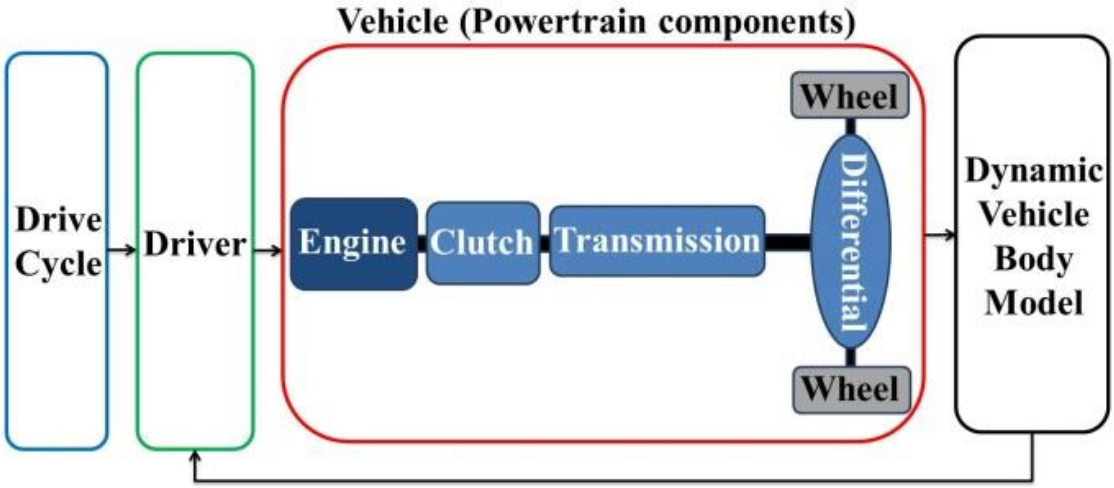

Figure 3-8: General forward-looking vehicle model

b) **Backward-looking:** In this approach, the required power is determined based on the known drive cycle data. Illustrated in Figure 3-9, this power demand is then calculated and transferred through the powertrain components to the engine or another main power source. Through this process and using the components' efficiencies, the power needed in each component is calculated. In this approach, the detailed dynamics of the components and the vehicle system is not considered; however, this will create less complicated models compared to the forward-looking models, which require solving differential equations.

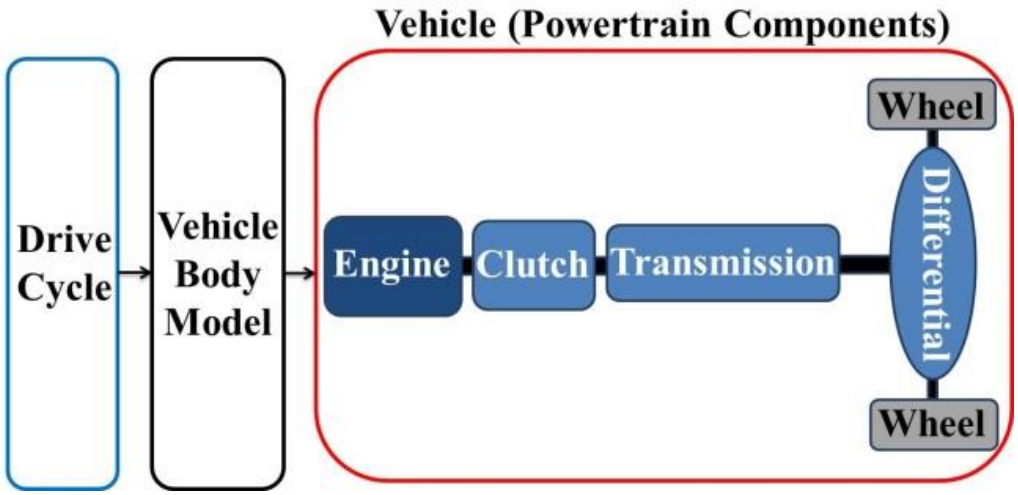

Figure 3-9: General backward looking vehicle model

Based on the fact that in this study, only the overall power consumption of the vehicle is of interest, the effects of vehicle dynamics due to the suspension can be safely ignored even though the model is not as realistic as the forward-looking model. The backward-looking approach modeling is chosen for this work to fulfill the purpose of optimization. Simultaneously, the developed vehicle model formulation is suitable for the power consumption objectives. The total system model consists of powertrain components (engine, bell housing, transmission, differential) and RAPS components (batteries, power electronic, generator, auxiliary load). The goal of this research is to design and optimize a suitable regenerative braking system, which can be added to a service vehicle's powertrain. As previously mentioned, the modifications to the vehicle powertrain should be kept to a minimum to make the changes affordable for the industrial purposes. Thus, there should not be any change to the configuration of the mechanical components of the vehicle. The powertrain components are modeled using the scalable backward-looking approach proposed by the Guzzella and Rizzoni [43]. In this approach, the actual consumed power of a

component is calculated by multiplying the required component torque and component current velocity given the component's efficiencies.

3.3.1 General Vehicle Model

In order to fulfill the need for a simple model for the backward-looking modeling approach, a simple vehicle body model is considered. This model only utilizes the drive torque, rolling resistance, and the resistive aerodynamic forces. The vehicle body model receives the demanded longitudinal velocity of vehicle (V_{Des}) and demanded longitudinal acceleration of vehicle (A_{Des}) as the input data. Based on these, the model calculates the torque (T_{Wheel}) and angular velocity (ω_{Wheel}) at the wheels (or axles) as follows:

$$\omega_{Wheel} = \frac{V_{Des}}{R_{Eff}} \tag{3-1}$$

$$T_{Wheel} = F_{Total}\, R_{Eff} \tag{3-2}$$

in which:

$$F_{Total} = F_{Drive} + F_{Drag} + F_{RR} \tag{3-3}$$

and

$$F_{Drive} = M_{Total}\ A_{Des} \tag{3-4}$$

$$F_{Drag} = \frac{1}{2} C_D\, \rho\, (V_{Des})^2\, A \tag{3-5}$$

$$F_{RR} = C_{RR}\, M_{Total}\ g \cos\alpha \tag{3-6}$$

where F_{Total}, F_{Drive}, F_{Drag}, and F_{RR} represents total vehicle longitudinal force, drive force, total aerodynamics drag force, and total tire rolling resistance force, respectively. C_D is the drag coefficient, ρ is the air density, A is the frontal area of vehicle, C_{RR} is the rolling

resistance of the tire, g is the gravitational acceleration, α is the road grade angle in radian, R_{Eff} is the effective tire radius, and M_{Total} is total vehicle mass, which is considered to be:

$$M_{Total} = M_{Veh} + M_{EES} + M_{Cargo} \tag{3-7}$$

where M_{Veh} is the vehicle mass before installing the EES packs or loading the cargo, M_{Cargo} is the cargo weight of the vehicle and M_{EES} is the mass of the electrical energy storage (EES) and other electrical parts. The total drive power demand (P_{Drive}), the power needed to move the vehicle, is equal to:

$$P_{Drive} = \omega_{Wheel} T_{Wheel} + P_{Lost} \tag{3-8}$$

in which P_{Lost} is the lost power in the powertrain system.

3.3.2 Final Drive (Differential)

The demand torque and angular velocity at the wheels (or axles) are the inputs for the final drive. After applying the final drive ratio (N_F), the demand torque (T_{DL}) and angular velocity (ω_{DL}) at the driveline are calculated as:

$$\omega_{DL} = N_F \omega_{Wheel} \tag{3-9}$$

$$T_{DL} = \frac{T_{Wheel}}{N_F \eta_F} \tag{3-10}$$

where η_F is the final drive efficiency.

3.3.3 PTO

The PTO consists of a set of gears that transfer the extracted mechanical power from the powertrain to the generator in the high power demand configuration. In order to keep the model as simple as possible, the PTO is modeled by a gear ratio (N_{PTO}) and an efficiency

factor (η_{PTO}). The modeling formula for the PTO defines its output torque ($T_{PTO-Out}$), which is equal to the generator torque in the high power demand configuration, and its output angular velocities ($\omega_{PTO-Out}$) as:

$$T_{PTO-Out} = (\frac{T_{PTO-In}}{N_{PTO}})\, \eta_{PTO} C_{Act-PTO} \tag{3-11}$$

$$\omega_{PTO-Out} = N_{PTO}\, \omega_{PTO-In} \tag{3-12}$$

in which $C_{Act-PTO}$ is the PTO activation control signal provided by the power management controller. In a high power demand configuration, the PTO is responsible for extracting the energy from the powertrain for the generator. This power extraction occurs in two general cases: i) Battery pack SOC decreases to a critical level where the power management controller decides to charge the battery pack (during the vehicle's movement or stop); and ii) regenerative braking. In either of the two general cases, the PTO's activation control signal will be one (active); otherwise this value will be zero (not active).

The power management controller, in general, controls the flow of power by monitoring the auxiliary power demand, battery state of the charge, vehicle status, brake pedal signal, and amount of power produced by the generator. Power management is considered as a higher level control algorithm that monitors the power flow between the vehicle powertrain, generator, and ESS as shown in Figure 3-10. The controller makes sure that the generator produces the maximum amount of power during regenerative braking to maximize the RAPS efficiency. In addition, the controller charges the batteries directly from the engine, during the peak engine performance, when the state of the charge is lower than a critical value.

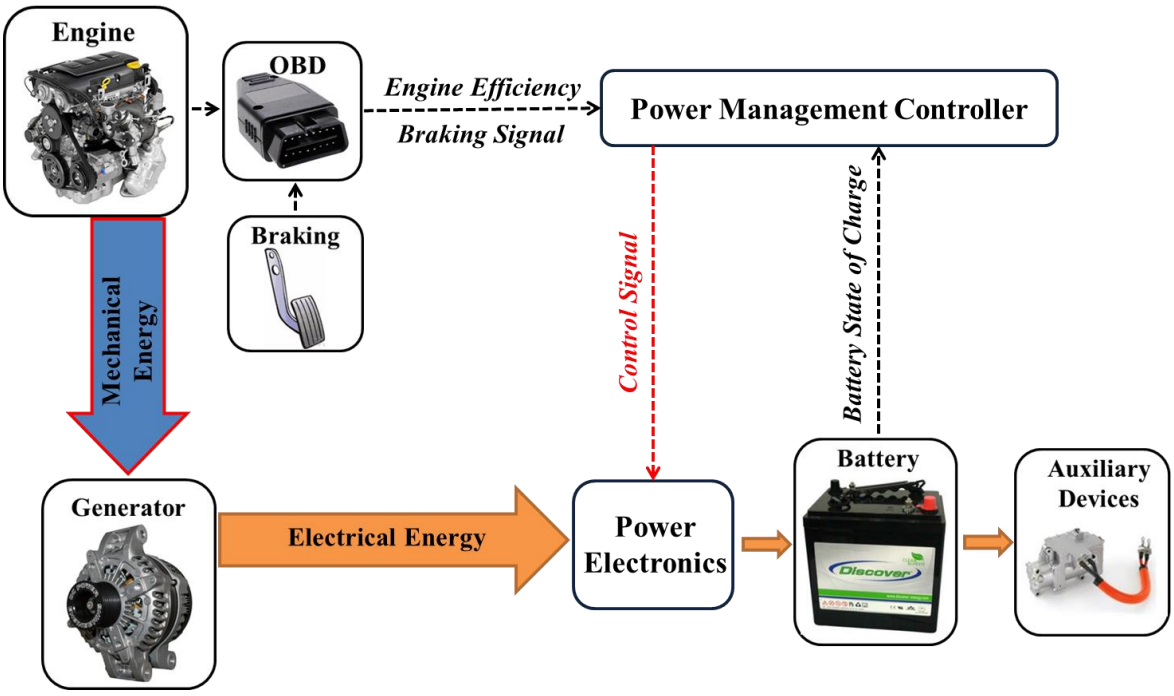

Figure 3-10: Power management controller input/output signals

In order to determine when to charge the batteries with the direct power from the engine, the controller considers the following criteria:

1. Once the SOC drops below the "High-level battery SOC threshold", the engine will be used to charge the battery packs if it is working at high efficiency (30% or higher);
2. Once the SOC drops below the critical value or "Low-level battery SOC threshold", the engine will be used to charge the battery packs under any condition, even low efficiency or idling, to prevent battery packs from any damage and life cycle reduction;
3. During braking conditions, there will certainly be no direct charging from the engine.

In order to make the system model as simple as possible, the controller utilizes a rule-based strategy that is adequate for control purposes in the design optimization of the proposed RAPS. The low and high-level battery SOC thresholds are defined in the optimization process, and will be further explained in Chapter 4.

3.3.4 Transmission (Gearbox)

The demand torque and angular velocity at the transmission output shaft (driveline) are the inputs to transmission model. After applying the transmission ratio (N_T), the demand torque (T_T) and angular velocity (ω_T) at the transmission are calculated as transmission model outputs:

$$\omega_T = N_T\, \omega_{DL} \tag{3-13}$$

$$T_T = \frac{T_{DL}}{N_T\, \eta_T} \tag{3-14}$$

in which η_T represents the transmission efficiency. The values of the transmission ratio are calculated using a look-up table indexed by the vehicle's longitudinal speed. It should be mentioned that the connection between the transmission and engine is provided by the bell housing (clutch / torque-convertor). Due to the fact that a simple component modeling approach is selected for this study, the effects of the bell housing part are considered in the transmission efficiency.

3.3.5 Generator

The output electrical power of the generator (P_G), in the form of output current (I_G) and output voltage (V_G) is calculated as:

$$P_G = I_G V_G = \eta_G T_G \omega_G \tag{3-15}$$

where the T_G and ω_G are the input torque and angular velocity to the generator, and η_G is the generator efficiency from the lookup tables indexed by the input torque and angular velocity to the generator. In the low power demand configuration, the generator is connected to the engine through the serpentine belt. During regenerative braking, the bell housing transfers braking powers from the transmission to the serpentine belt. In this case:

$$T_G = \frac{\alpha_{Reg} T_T}{N_G} \tag{3-16}$$

$$\omega_G = N_G \omega_T \tag{3-17}$$

in which α_{Reg} is the regenerative braking coefficient and N_G is the generator ratio due to serpentine belt pulleys. During braking conditions (due to safety, general limitations of adding regenerative braking, system efficiency, and size limitation of the generator), conventional mechanical brakes still work. Therefore, by adding regenerative braking to the vehicle, just a percentage of the braking torque energy can be captured by the generator. The regenerative braking coefficient (α_{Reg}) represents this percentage. On the other hand, during vehicle movement or vehicle stop scenarios, the generator demanded torque, which is determined by the controller as it charges the battery in a critical level SOC, will be provided by the engine. In these cases:

$$T_G = \frac{T_{E\_Charge}}{N_G} \tag{3-18}$$

$$\omega_G = N_G \omega_E \tag{3-19}$$

where T_{E_Charge} is the engine demand torque for direct battery charging conditions (when the generator is run by the engine instead of regenerative breaking energy). In these scenarios, the engine demanded torque for direct charging (T_{E_Charge}) will be added to the transmission demanded torque (T_T) and the required torque to overcome the resistance forces at the engine (T_R) in order to determine the total demand torque from the engine (T_E):

$$T_E = T_R + T_T + T_{E_{Charge}} \tag{3-20}$$

$$\omega_E = \omega_T \tag{3-21}$$

Based on the fuel consumption rate during idling, the engine idling torque is estimated and this value is considered to be the needed torque to overcome the engine resistance forces (T_R).

In the high power demand configuration, a generator is connected to the PTO. Therefore, generator torque and angular velocity are equal to the output torque of the PTO ($T_{PTO-Out}$) and output angular velocities of the PTO ($\omega_{PTO-Out}$), respectively. When considering the "Transmission Aperture" PTO configuration in the regenerative braking phase, the generator torque and angular velocity are determined as:

$$T_G = (\frac{\alpha_{Reg} T_T}{N_{PTO}})\, \eta_{PTO} C_{Act-PTO} \tag{3-22}$$

$$\omega_G = N_{PTO} \omega_T \tag{3-23}$$

During vehicle movement or vehicle stop scenarios, if the battery SOC decreases to the critical level, the generator will be powered directly by the engine (direct battery charging). In these scenarios, the generator torque is calculated as:

$$T_G = \left(\frac{T_{E\_Charge}}{N_{PTO}}\right) \eta_T \eta_{PTO} C_{Act-PTO} \tag{3-24}$$

$$\omega_G = N_{PTO} \omega_E \tag{3-25}$$

Similarly, in the low power demand configuration, for the direct battery charging condition in the "Transmission Aperture", the PTO configuration equations (3-20) and (3-21) are valid.

3.3.6 Engine

The engine model should be scalable so that the developed model can be easily modified for different vehicles. Similar to the model used in [43], the applied engine model in this study has the scalability and composability features. Using a scalable model, the vehicle components that belong to the same class (for example ICEs) can be modeled using the same basic model. The important factor is that the model should be independent from the component size and can be scaled based on a simple scalar variable such as displacement or power rating. The composability feature is concerned that the system components' model can easily compose the other related parts.

Storing, converting, and transferring the energy in a vehicle is concerned with three domains: chemical, mechanical, and electrical. In each energy domain, power is equal to the product of flow variable and effort variable. In the powertrain analysis, angular velocity and torque are the flow and effort variables, respectively [44]. The Willan's line modeling approach, which is proposed by Rizzoni et al. [49], normalizes the flow and effort variables to create a model that is independent of scaling. The Willan's line concept for a generic energy converter, ICE in this case, is shown in Figure 3-11.

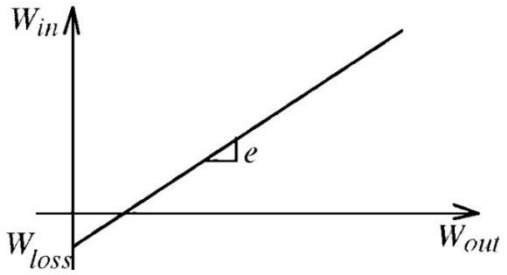

Figure 3-11: Willan's line modeling concept [43]

This approach relates the available input energy for conversion ($\boldsymbol{W_{In}}$), to the actual useful output energy of the converter ($\boldsymbol{W_{Out}}$) as follows:

$$W_{Out} = eW_{In} - W_{Loss} \tag{3-26}$$

where in an ICE, e is the energy conversion efficiency that is characteristic of a specific cycle (Otto, Diesel, etc.), and W_{Loss} is the total power loses in the energy converter. As illustrated in Figure 3-11, this relation has the appearance of a straight line, which gives Willan's line its name [43]. By defining the efficiency of the energy converter (η) as the ratio of actual useful output energy (W_{Out}) to the available input energy (W_{In}) and substituting equation (3-26), the efficiency ratio η becomes:

$$\eta = \frac{W_{Out}}{W_{In}} = \frac{eW_{In} - W_{Loss}}{W_{In}} = e - \frac{W_{Loss}}{W_{In}} \tag{3-27}$$

It is obvious that "*the actual conversion efficiency is a function of the operating conditions of the converter*" [43], and this efficiency will be maximized when the ratio of energy losses to input energy is minimized. In a general ICE, the following equation is valid [43]:

$$\omega_E T_E = \eta_E P_{Fuel} = \eta_E \dot{m}_F H_L \tag{3-28}$$

in which P_{Fuel} represents the enthalpy flow associated with the fuel mass flow, η_E is the engine efficiency, $\dot{m}_F$ is the fuel mass flow, and H_L is fuel's lower heating value. In equation (3-28), engine efficiency is defined based on dimensional variables that depend on the engine's size. In order to develop a scalable engine model, which is independent of the power rating or displacement and can be used for size optimization, Willan's line scalable engine model is utilized to calculate the engine efficiency. As proposed by Guzzella and Rizzoni [43], [44], using normalizations based on the ICE's characteristics, this dependency can be avoided.

In this approach, the scalable model of the engine is developed based on three parameters: i) The mean effective pressure (p_{ME}), which describes the engine's ability to produce mechanical work, ii) Mean piston speed (V_{MP}), which represents engine's operating speed, and iii) Fuel available mean effective pressure (p_{MF}), which is the maximum mean effective pressure produced by an engine with 100% efficiency utilizing a unit fuel [43]. In the steady-state running condition of the engine, p_{ME}, V_{MP} and p_{MF} are calculated based on the following equations [43]:

$$p_{ME} = \frac{N\,\pi}{V_{ED}}\,T_E \tag{3-29}$$

$$p_{MF} = \frac{N\,\pi\,H_L}{V_{ED}}\,\frac{\dot{m}_F}{\omega_E} \tag{3-30}$$

$$V_{MP} = \frac{S}{\pi}\,\omega_E \tag{3-31}$$

In these equations, S represents the engine's stroke, and V_{ED} represents the engine's displacement (volume). For a four-stroke engine, N is equal to 4, and for a two-stroke engine,

N is equal to 2. By considering equations (3-28), (3-29), and (3-30), engine efficiency (η_E) can be defined as:

$$\eta_E = \frac{p_{ME}}{p_{MF}} \tag{3-32}$$

Based on the concepts of thermodynamic efficiency and internal losses during the engine cycle, the mean effective pressure (p_{ME}) is calculated as:

$$p_{ME} = e_E\, p_{MF} - p_L \tag{3-33}$$

in which e_E is the thermodynamic properties of the engine related to the mean effective pressure, and p_L is the engine losses where:

$$p_L = p_{LG} + p_{LF} \tag{3-34}$$

In this equation, p_{LG} represents the engine's losses due to gas exchange, and p_{LF} represents the engine's losses due to friction. According to [45], p_{LF} can be estimated as:

$$p_{LF} = k_1(k_2 + k_3(S\omega_E)^2)\, \Pi_{max} \sqrt{\frac{k_4}{B}} \tag{3-35}$$

where B is the engine cylinder bore, Π_{max} is the maximum boost pressure, and k parameters are experimental parameters. Using equations (3-32), (3-33), (3-34), and (3-35), η_E is determined. Also, the fuel consumption can be calculated for a given engine output torque and speed.

In the model developed in this study, the engine model receives the demand torque and angular velocity as the inputs. The engine efficiency (η_E) is calculated based on the aforementioned method, and sent to the controller as the engine model output. Also, based on

equation (3-28) and η_E value, the required fuel (fuel mass flow of $\dot{m}_F$) can be calculated as the second output of the engine model as follows:

$$\dot{m}_F = \frac{\omega_E T_E}{H_L \eta_E} \tag{3-36}$$

3.3.7 Electrical Energy Storage Systems (Batteries)

There are different electrical components in the proposed vehicle. For some of these components, such as a plug-in charger or converters, a simple algebraic model is used. The EES system is the main electrical part whose impact on the system is important. The EES module stores the generator output energy during regenerative braking or direct charging from the engine. In addition, the module feeds the auxiliary devices during their operation time. There are different types of rechargeable batteries on the market and new types with better technologies are introduced every year. An accurate model of a battery is complicated and is not necessary for the problem presented in this thesis. Generic knowledge of battery behavior can be sufficient for modeling purposes in electrical and hybrid vehicles. Therefore, in the EES modeling process, the exact chemical reaction or other related changes are not considered; however, the changes in the energy and power level are modeled. Generally, in the literature, battery models are categorized into three main groups: experimental, electrochemical, and electric circuit-based. Among them, the electric circuit-based modeling approach will adequately fulfill the battery modeling needs in electrical and hybrid vehicles with acceptable accuracy [46]–[48].

If considering the electric circuit-based modeling approach, there are different models developed for the batteries. A comparison among seven common circuit-based models is

presented in [46]. It is concluded that “Dual Polarization (DP)” and “Thevenin” models perform best since the impact of the battery relaxation effect is considered for their modeling. As illustrated in Figure 3-12, both Dual Polarization and Thevenin models are based on a simpler model known as internal resistance model or “Rint”.

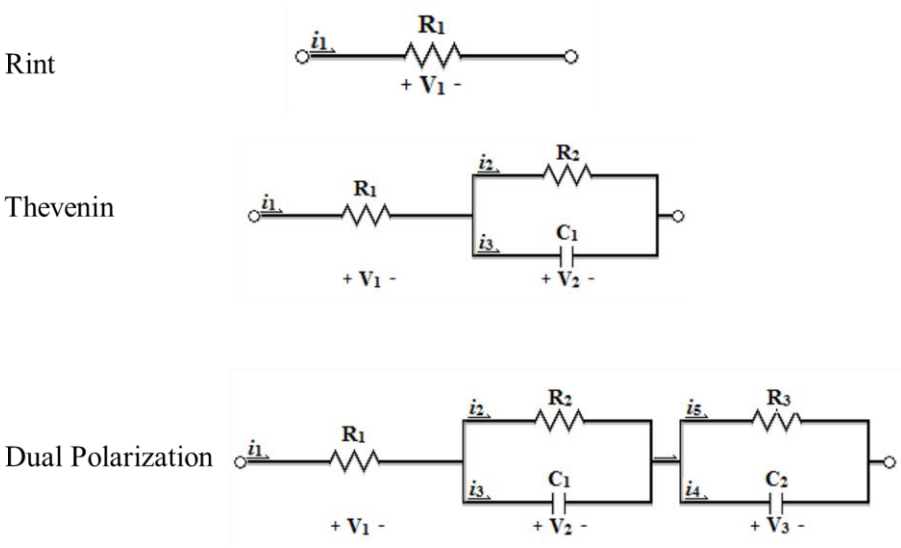

Figure 3-12: Common electric circuit-based models for batteries [49]

The “Thevenin” model is created by adding an RC network to the “Rint” model and “Dual Polarization” is created by adding an RC network to the “Thevenin” model. Each RC network consists of a resistor (R) and a capacitor (C). In Figure 3-12, R_1, R_2, and R_3 represent the effect of the series resistance, long time transient resistance, and short time transient resistance of the battery, respectively. In addition, V_1, V_2, and V_3 represent the terminal voltage, long time transient voltage, and short time transient voltage of the battery, respectively. Finally, C_1 and C_2 represent the long time transient capacitance and short time transient capacitance of the battery, respectively. It should be considered that in the “Thevenin” model, the set of C_1, V_2, and R_2 are just considered as the representatives of the

transient time changes. However, in the “Dual Polarization” model the set of C_2, V_3, and R_3 is added to represent the short time transient changes and the set of C_1, V_2, and R_2 represent the long time transient changes.

It is possible to add more RC networks to the “Rint” model; however, adding more RC networks increases the complexity and computational cost of the model without improving model accuracy. On the other hand, based on experiments performed by [46] and [50], adding more than two RC networks decreases the performance of some aspects of the model.

According to [46], the “Dual Polarization” model performs best among common electric circuit-based battery models followed by the “Thevenin” model. However, both of these models are created based on the “Rint” model, and considering experimental results [46], [49], the performance of the “Rint” model is close to the performance of the “Dual Polarization” and the “Thevenin” models, especially considering the interests and conditions of this study. From [46], the maximum error in the Hybrid Pulse Power Characterization (HPPC) tests [51] for a battery cell with nominal voltage of 3.2 V, is less than 40 [mV](1.25%) for the “Dual Polarization” and the “Thevenin” models, and less than 180 [mV] (%5) for the “Rint” model; however, the mean error for all three models is less than 10 [mV] (0.3%).

The “Thevenin” and “Rint” models are compared in [55]. The comparison shows that in a city drive cycle such as the UDDS, which is the main part of service vehicles working drive cycle, the difference between two battery models is small. This is similar to the results of [52], where it is considered that the “Rint” model has a performance error around 5% compared to “Thevenin” model. Therefore, although the battery’s dynamic voltage

performance is ignored in the “Rint” model, in the working condition of service vehicles, the performance of the “Dual Polarization”, the “Thevenin”, and the “Rint” models are close. Due to this fact and considering that one of the main objectives of this research is to develop a method that can be easily used to design RAPS for different service vehicles, the “Rint” model is selected for battery modeling. This model will not increase the computational cost. More importantly, it does not need different battery parameters, such as C_1, C_2, V_2, V_3, R_3, and R_3, which are generally not provided by the battery manufacturer. There is a need for performing characterization tests such as HPPC [51] to identify these parameters. This process is not of interest in RAPS design for different service vehicles and the fleet companies.

3.3.7.1 Rint Battery Model

In this model, current is calculated by considering the internal resistance when calculating the charge and discharge power of the battery. During battery charge and discharge, the desired change in the stored power and energy of the battery (P_{B_Desired}) can be determined as:

$$P_{B\_\text{Desired}} = R_{In} I_B^2 + V_{B\_OC} I_B \tag{3-37}$$

in which R_{In} , I_B, and V_{B_OC} represent the internal resistance, current, and the open circuit voltage of the battery, respectively. It is assumed that when the battery is being charged, the current and the subsequent desired change in the battery power (P_{B_Desired}) are both positive. Conversely, when the battery is being discharged, the current and the desired change in the battery power (P_{B_Desired}) are both negative. It should be mentioned that the first term of equation (3-37), $R_{In} I_B^2$, is representing the lost energy due to internal resistance of the

battery. Generally, the energy losses are much smaller when compared to the second term of equation (3-37), $V_{B\_OC}I_B$. Hence, the sign of the P_{B_Desired} in equation (3-37) will follow the sign of the second term and the current. Solving equation (3-37) for I_B, there are two solutions for battery current as:

$$I_B = \frac{-V_{B\_OC} \pm \sqrt{{V_{B\_OC}}^2 + 4P_{B\_\text{Desired}}R_{In}}}{2R_{In}} \tag{3-38}$$

In order to determine the correct solution, it is assumed that in the ideal condition, there is no waste of energy in the internal resistance of the battery; thus, equation (3-37) will change to the ideal form of:

$$P_{B\_Desired} = V_{B\_OC\_Ideal}I_{B\_Ideal} \tag{3-39}$$

and from that:

$$I_{B\_Ideal} = \frac{P_{B\_Desired}}{V_{B\_OC\_Ideal}} \tag{3-40}$$

in which $V_{B\_OC\_Ideal}$ and I_{B_Ideal} are the open circuit voltage and current of the battery in the ideal condition, respectively. According to the assumption for the ideal condition, I_{B_Ideal} is the maximum possible absolute value for battery current. Considering the solutions of equation (3-38), the larger value of the two solutions is higher than the I_{B_Ideal}; hence, this higher value cannot be accepted.

The battery open circuit voltage (V_{B_OC}), is a function of the battery SOC. In order to model the related changes of the SOC and the battery open circuit voltage, a look-up table is utilized. Finally, based on the calculated current and open circuit voltage, the actual charge and discharge power of the battery (P_{B_Actual}) is defined as:

$$P_{B\_Actual} = V_{B\_OC} I_B \tag{3-41}$$

By integrating these actual charge and discharge powers of the battery through time, the change in the battery energy and therefore the SOC level of the battery at each sample time can be determined.

It should be mentioned that desired battery charge and discharge power ($P_{B\_Desired}$), is the amount of energy that is sent to the battery through the generator during charging or the amount of energy demanded and desired from the battery during discharging. However, comparing equations (3-37) and (3-41), the desired power is not equal to the actual power. During charging, I_B>0, the actual power reserved in the battery that can be used later (P_{B_Actual}) is lower than the expected and desired power ($P_{B\_Desired}$) because of the wasted energy by the battery's internal resistance ($R_{In} I_B^2$). During discharging, I_B<0, the absolute value of the actual power received from the battery (P_{B_Actual}) is lower than the demanded power ($P_{B\_Desired}$) again because of the wasted energy by the battery's internal resistance. Therefore, in all conditions:

$$\left|P_{B\_Actual}\right| \leq \left|P_{B\_Desired}\right| \tag{3-42}$$

The equality happens when the ideal condition is considered.

3.3.7.2 Selected battery packs specifications

Among the various types of batteries that are used in electric and hybrid vehicles, the most common examples are lithium-ion, lead-acid, and nickel-metal-hydride batteries. The chosen batteries for this study and their important characteristics for the purpose of this study are explained in this subsection. For this research, different models of lithium-ion and lead-acid

batteries are considered in order to find the best solution for the proposed RAPS. The specifications and acceptable DOD of the chosen battery packs (for their life cycles to last at least 5 years) are presented in Table 3-1. For dry-cell and lithium-based battery packs to last at least 5 years, the value of the DOD should be less than 30% and 70 %, respectively, given 260 active work day a year in Canada by Statistics Canada [52].

According to Table 3-1, it can be seen that the selected battery packs for optimization have a wide range of capacity, weight, and price. It should be noted that for the first four rows of Table 3-1, the selected batteries are available in prepackaged conditions to match the regular vehicle's electrical system of 12V (or 24V). Hence, for the remaining battery models, a set of four series cells is considered to have almost the same nominal voltage for all of the chosen battery packs. Due to this fact, the number of parallel row of battery cells will be used as the optimization variable for battery packs' size optimization, and the output voltage of ESS remains around 12V. Based on suggestions of the project's industrial partners targeted service vehicles for this project has the electrical system's voltage of 12V. Therefore, in order to simplify the optimization process and make it easier to compare between different battery packs, it is considered that in all the configurations the nominal voltage of the EES is around 12 V. This voltage is considered for simulation and HIL testing purposes and can be adjusted to any other voltage depending on the generator, service vehicles' auxiliary devices operating voltage and converters. It should be noted that the Original Equipment Manufacturer (OEM) battery will not be considered to power the auxiliary devices.

Table 3-1: Chosen battery packs for optimization

Battery Type	Nominal Voltage [V]	Capacity [kWh]	Capacity [Ah]	Weight [Kg]	Price [$/Unit]	Acceptable DOD [%]
EV12_140X DiscoverDryCell	12	1.68	140	50	490	DOD < 30%
EV12_180X DiscoverDryCell	12	2.172	181	60	585	DOD < 30%
EV12_8DA_A DiscoverDryCell	12	3.2	260	82	740	DOD < 30%
EV12_Li_A123 ALM12V7	13.2	0.06	4.6	0.85	125	DOD < 80%
EV12_Li_A123 ANR26650	13.2	0.029	2.3	0.35	18	DOD < 80%
EV12_Li GBS_100Ah	12.8	1.28	100	12.8	555	DOD < 80%

3.3.7.3 Battery Life Cycle

It is assumed that the designed RAPS should work in service vehicles for a duration of 5 years before the batteries need to be changed. This duration obviously depends on the type of EES could be adjusted. Therefore, all the cost calculations in the optimization part (Chapter 4) are based on a five-year interval. It is essential to consider the battery life cycle in the design process in order to ensure that the EES has acceptable performance for the expected working time. During the five-year interval considered for the optimization, the system will have a high number of charge and discharge cycles. As such, it is important to consider the degradation and useful life cycle of the battery packs. There are different definitions for battery life cycle, all of which consider the number of cycles that a battery can have where its performance stays close to its original condition. For instance, considers the original condition to be where the nominal capacity is higher than 80% of the initial rated capacity. When calculating a battery life cycle, the number of complete cycles (battery fully charged and discharged) should be considered. During a complete battery cycle, all of the battery's power should be used; however, this can happen in more than one charging-discharging

process. The number of charge-discharge cycles, depth of discharge (DOD), temperature and time are the main factors affecting the battery life cycle.

It is important to calculate the number of complete cycles in the battery pack for each active day of a service vehicle, and based on these values, it is important to limit the optimization boundary limits for the optimization variables. The variables of low and high-level battery SOC thresholds must be optimized in order to select a correct battery model that can last for the estimated 5 years. The number of complete cycles can be defined as:

$$Life - Cycle_{Per-Day} = \frac{0.5\left[\left(\sum_{TS=1}^{n} |SOC_{TS} - SOC_{TS-1}|\right) + SOC_{charge}\right]}{100} \quad (3\text{-}43)$$

in which the $Life - Cycle_{Per-Day}$ is the total number of complete charge-discharge cycles for each simulation day, SOC_{TS} is the battery pack SOC level in the time step number TS, n is the total number of time steps, and SOC_{charge} is the total SOC change during the overnight plug-in charging.

It is considered that at the end of the day, the service vehicle will be returned to a specific station that has the accessories to recharge the batteries up to 95% of their capacities during the night. Thus, it is assumed that the battery pack is in the same SOC level at the beginning of each day, so the amount of charge and discharge are equal during one complete day. Total charge/discharge in one-day simulation is equal to half of the total absolute change in the SOC level, which is the summation of the absolute value of all the SOC level changes between the time steps of the simulation plus the amount of charge received from the plug-in electricity during one overnight charge, SOC_{charge}. In order to calculate the SOC_{charge}, the final SOC level of battery pack at the end of working day is recorded as SOC_{final}. The

change in the SOC level of the battery pack during overnight plug-in charging can be calculated as:

$$SOC_{charge} = 95 - SOC_{final} \tag{3-44}$$

The final SOC of all working days will be the same since the SOC starts from the same level of 95% each day and same drive cycle is used for each working day.

Chapter 4

Multi-disciplinary Design Optimization and Case Studies

4.1 Introduction

This chapter will describe the process of the multi-disciplinary design optimization. Since the goal of this study is to perform the least amount of changes in the existing vehicle system, no option is considered for the optimization of the existing parts of the vehicle drivetrain. In this report, two optimization methods (genetic algorithm (GA) and simulated annealing (SA)) are considered since they are suitable for discrete and derivative free problems and have the ability to find the optimal solution. These two techniques are briefly discussed in Appendix A.

4.2 Optimization Process Review

The goal of component modeling was to study the energy and power efficiencies and flow in the system. Therefore, a backward-looking modeling approach is utilized to compute the vehicle power consumption and the overall efficiency with a minimum computing cost and acceptable accuracy.

Each component of the vehicle model system such as the engine, battery, and generator, as well as the controller's power management logic is considered as an individual discipline. Hence, the MDO process should be utilized to simultaneously optimize the component sizing and power management logic in the overall system.

4.2.1 Optimization Algorithm Structure

MATLAB software is utilized for the optimization process since the vehicle's component models are developed in MATLAB and Simulink software. As illustrated in Figure 4-1, the whole process is performed by running three steps:

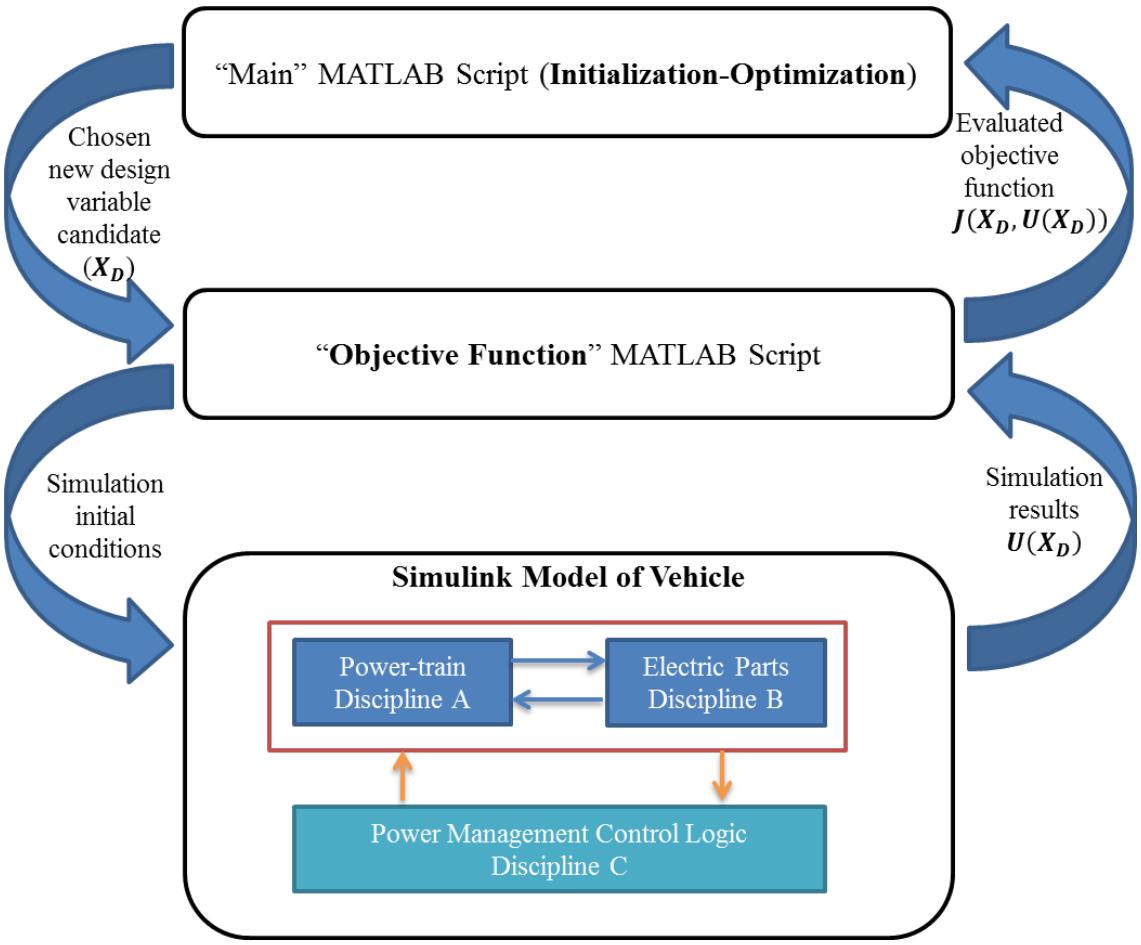

Figure 4-1: Optimization software scripts

1- "Main" MATLAB script: Initialization parameters and optimization process are applied in this step. The upper and lower bounds of the design variable candidates, namely vector X_D, and the optimization algorithm are defined. As shown in Figure 4-2, at each iteration, the optimizer will choose a new X_D that contains

optimization variables such as the powertrain component size and power management logic. This X_D should satisfy the optimization constraints, $C(X_D)$. The "main" script also receives evaluated objective function $\left(X_D, U(X_D)\right)$, and subsequently investigates the terminating conditions to stop the process.

2- "Objective function" MATLAB script: The chosen X_D will be sent to this script. Based on X_D, the initial conditions for the simulation will be updated. In addition, the results of the simulation ($U(X_D)$) will be transferred to this script in order to evaluate the objective function value, which will be further explained in the next subsection.

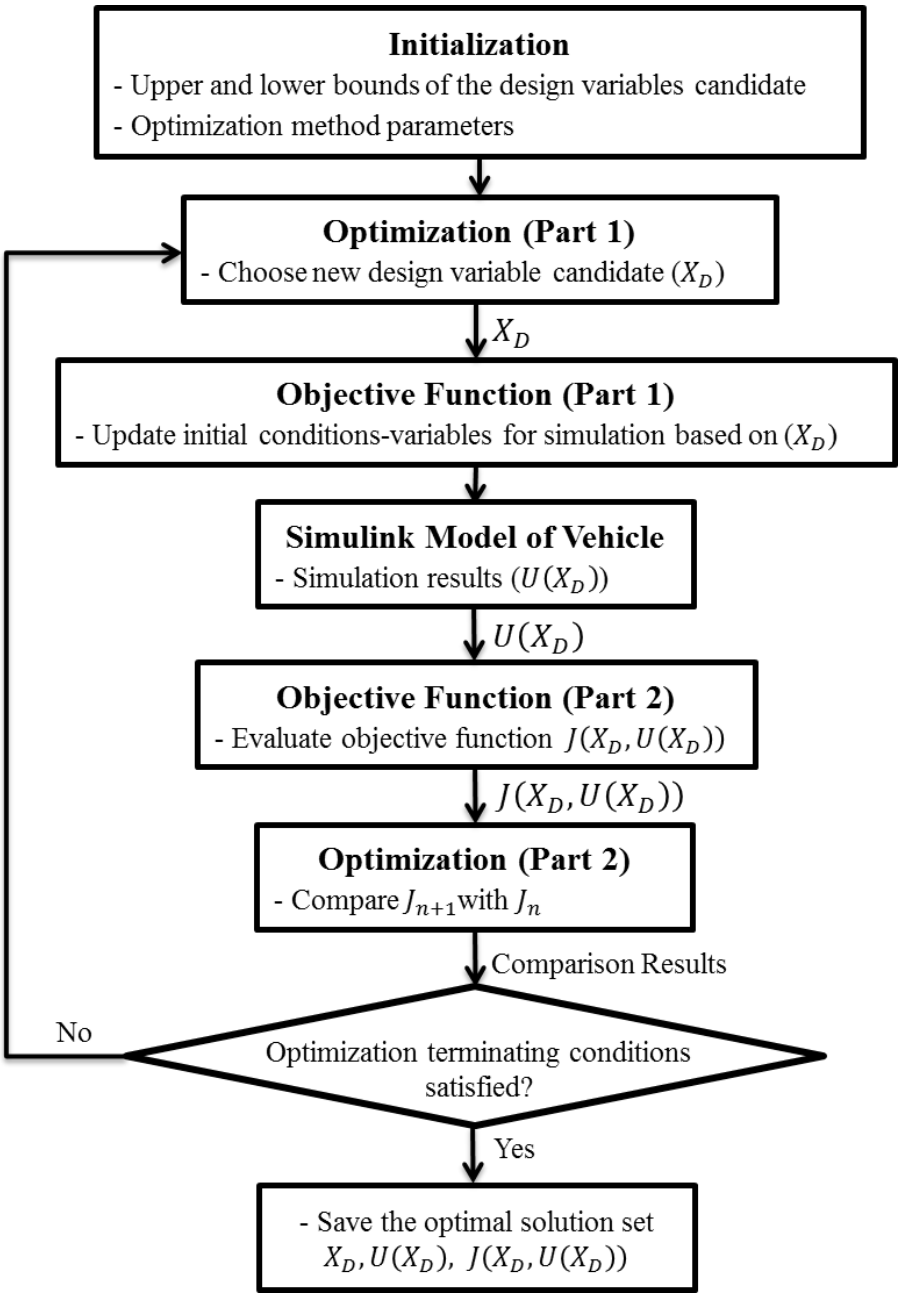

Figure 4-2: Optimization process

3- Simulink model of the total vehicle: This model consists of various disciplines, and it calculates the energy consumption of the vehicle in the form of fuel and electricity consumption.

4.3 Objective Cost Function

In this study, the main goal is to find the lowest total system cost or highest saving by utilizing the RAPS. The cost function should consider the capital and running costs of the RAPS over a given period of time. The optimizer objective function is defined from a financial cost perspective, where the objective is to minimize:

i) the initial cost of batteries and the added accessories to the existing vehicle,

ii) the cost of fuel consumption for running the service devices (like AC or refrigeration system),

iii) the plug-in electricity consumption over a specific period.

The design challenge lies in balancing the size and cost of the battery and other added parts against the cost of the engine's fuel and plug-in electricity consumption for running the service devices.

According to the life cycle of regular battery packs in electrical and hybrid vehicles, it is considered that a battery pack can last for about 5 years [37], [53]–[57]. Moreover, in order to make an assumption for the number of days per year as the working condition of a service vehicle, the general idea of a 260-day work year in Canada by Statistic Canada [52] is used.

In the optimization process, the optimizer tries to determine the best battery pack size and the most appropriate power management logic (low and high-level battery SOC thresholds) in order to minimize the objective function $J\left(X_D, U(X_D)\right)$, which is defined as:

$$Minimize\ J\big(X_D, U(X_D)\big)\ ;\quad w.r.t\ X_D \tag{4-1}$$

$$Considering\ Constrain\ C(X_D)$$

in which optimization variables (design variable candidates or X_D) are the number of battery packs, low level battery SOC thresholds, and high level battery SOC thresholds. The function $U(X_D)$ consists of Simulink model outputs. The constraints vector $C(X_D)$ represents the equality and inequality constraints of the problem.

The objective function J is the total financial amount of the system and energy consumptions, without considering the cost of the existing vehicle, and it is calculated over a period of five years with a 260-day work year. Different parts of objective function are explained in the following subsections and the total objective function equation is presented in Subsection 4.3.4 .

4.3.1 Fuel Costs

One of the benefits of using the Willan's line engine model is that this model can provide a good estimation of the consumed fuel based on the fuel energy density. Utilizing equation (3-36), at each time step based on the value of the engine efficiency (η_E), the fuel heating value (H_L), the engine torque (T_E) and the engine angular velocity (ω_E), the value of the fuel mass flow ($\dot{m}_F$) can be calculated. Adding these values over time will result in the total fuel consumption of the vehicle during each drive cycle (active day). Total fuel consumption of the vehicle, $F\big(U(X_D)\big)$, through the desired optimization process can be calculated as:

$$F\big(U(X_D)\big) = Total\ Fuel\ cost = \left[\sum_{t=0}^{T} Fuel_{Consumed} \times (Fuel_{Cost})\right] \times Days_{Active} \times Years \tag{4-2}$$

in which t is the vehicle model simulation time, T is the total time of simulation or drive cycle, and term $\sum_{t=0}^{T} Fuel_{Consumed}$ represents the total fuel consumption through one day (or one simulation). $Fuel_{Cost}$ is the unit price of fuel (in this study per liter gasoline), $Days_{Active}$ is the number of active days per year, and $Years$ represents the targeted active years for the optimizer. Equation (4-2) can be simplified as:

$$F\big(U(X_D)\big) = Fuel_{Cost} \times Days_{Active} \times Years \times f\big(U(X_D)\big) \tag{4-3}$$

in which $Fuel_{Cost}$, $Days_{Active}$, and $Years$ are constant values and $f\big(U(X_D)\big)$ represents the total fuel consumption through one active day or simulation which is a function of $U(X_D)$, Simulink model outputs.

4.3.2 Plug-in Electricity Cost

It is considered that at the end of the day, the service vehicle will return to the specific station, which has the accessories to recharge the batteries up to 95% of their capacities during the night. The total consumed electrical energy during the night can be calculated based on the change in the SOC level of the battery pack during overnight plug-in charging (SOC_{charge}). Final SOC of all working days will be the same since the SOC starts from the same level of 95% each day and the same drive cycle is used for each working day. Based on equation (3-44), the total consumed electrical energy during each night can be determined as:

$$p\big(U(X_D)\big) = Plug\_In_{Energy} = 0.001 \times 0.01 \times \big(SOC_{charge} \times Capacity_{Total} \times V_{B\_Charge}\big) \tag{4-4}$$

where $Plug\_In_{Energy}$ is the total kWh consumed electrical energy during each night, $Capacity_{Total}$ is the total capacity of ESS (or the battery packs in this study), and V_{B_Charge} is the charging voltage of the battery pack which is one of the battery's specifications. The

value of $Capacity_{Total}$ is based on watt-hours [Wh] in order to find the value of $Plug\_In_{Energy}$ in kWh, which is the based price calculation unit, and the coefficient 0.001 is added in equation (4-4). The coefficient 0.01 is added to change the value of SOC_{charge} from present to the acceptable ratio for energy consumption. The total plug-in electricity consumption, $P\big(U(X_D)\big)$, is defined as:

$$P\big(U(X_D)\big) = Plug\_In_{Cost-Total} = \big[Plug\_In_{Energy} \times Electricity_{Cost}\big] \times Days_{Active} \times Years \quad (4\text{-}5)$$

in which the $Electricity_{Cost}$ is the price of purchased kWh electricity during the night hours. Equation (4-5) can be simplified as:

$$P\big(U(X_D)\big) = Electricity_{Cost} \times Days_{Active} \times Years \times p\big(U(X_D)\big) \quad (4\text{-}6)$$

in which $Electricity_{Cost}$, $Days_{Active}$, and $Years$ are constant values and $p\big(U(X_D)\big)$ represents the total purchased electrical energy during each night after one active day, which is a function of $U(X_D)$ and depends on model outputs.

4.3.2.1 Battery Cost Function

Battery packs are usually the most expensive electrical component in electrical and hybrid vehicles. The price of each battery bank is presented in Table 3-1. The optimizer will determine the number of parallel set of each of these priced battery banks. The total cost of the ESS system (battery pack) can be calculated as:

$$B(X_D) = \ Total\ Battery\ cost = Battery_{Banks} \times Battery_{Cost} \quad (4\text{-}7)$$

where $Battery_{Banks}$ is the number of parallel set of battery banks (determined by the optimizer), and $Battery_{Cost}$ is the unit price of each battery bank.

4.3.3 Initial RAPS Components' Costs

Other than the cost of battery packs, there are other initial costs. Due to lack of information, the maintenance cost, initial costs, and added weight of these added parts, which are mostly belongs to the EES system, are estimated based on the available online data and vehicle parts dealer websites. Assumptions for the price of added initial parts are presented in Table 4-1.

Table 4-1: Estimated Prices for Added Initial Parts

Added Component	2.5 kW Generator	Lithium-Based Battery Packs Accessories	Deep Cycle Battery Packs Accessories
Estimated Price [$]	300	3100	1500

Due to the sensitivity of lithium-based batteries to the temperature and overcharge conditions, utilizing these kinds of batteries results in the use of more expensive power management control and plug-in chargers. This extra cost will be compensated by their lower weight to capacity factor and their better DOD limitations.

4.3.4 Total Objective Function

The objective function J is defined based on the total cost of the system and energy consumptions without considering the cost of existing vehicle. This function is the summation of the fuel cost, plug-in electricity cost, initial cost of battery packs, and initial cost of added accessories. Considering the discussions in Subsections 4.3.1, 4.3.2, 4.3.2.1, and 4.3.3, the objective function can be defined as:

$$J = \left[\left(\sum_{t=0}^{T} Fuel_{Consumed} \times Fuel_{Cost}\right) + \left(Plug\_In_{Energy} \times Electricity_{Cost}\right)\right] \times Days_{Active} \times Years + Battery_{Banks} \times Battery_{Cost} + Accessory_{Cost} + 10^{9} ERROR \quad (4\text{-}8)$$

in which term $10^9 ERROR$ is either a zero or a large number to control the solution of the optimizer. If $ERROR$ is zero the solution is acceptable, if not, such as when the demanded power is more than the maximum available engine power, $10^9 ERROR$ takes a large number to prevent the optimizer from selecting a solution. All of the variables of equation (4-8), and their values in this study are explained in Table 4-2. The objective function J can be rearranged as:

$$J\left(X_D, U(X_D)\right) = a_1 F\left(U(X_D)\right) + a_2 P\left(U(X_D)\right) + a_3 B(X_D) + b_4 + E \quad (4\text{-}9)$$

in which a_1, a_2, and a_3 represent the optimization weighting coefficients for the fuel consumption, plug-in electricity and battery pack, respectively. b_4 models the capital cost of the system, which is the accessory costs, and E represents the error signal preventing the optimizer from selecting impossible solutions. Considering the fact that all the values in equation (4-8) are normalized to the actual dollar values, the optimization weighting coefficients (a_1, a_2, and a_3) in equation (4-9) are equal to one. In should be noted that these coefficients can be modified based on new consideration for the optimization such as air pollution or battery degradation.

Table 4-2: Optimization variables description (related to equation (4-8))

Variable	Definition	Value
t	Vehicle model simulation time	Based on drive cycle
T	Total time of vehicle model simulation or drive cycle	Based on drive cycle
$\sum_{t=0}^{T} Fuel_{Consumed}$	Total fuel consumption through one active day (or one complete simulation-drive cycle)	Based on the drive cycle and fuel consumption rate from Willan's line model of engine
$Fuel_{Cost}$	The unit price of fuel	In this study, 1.5 $ per liter gasoline
$Plug\_In_{Energy}$	Total kWh consumed electrical energy during each night from plug-in	Calculated from equation (4-4) with respect to the value of ESS capacity and voltage, and the change in the SOC level of ESS
$Electricity_{Cost}$	Price of purchased kWh electricity during the night hours	In this study, 0.14 $ for each kWh based on off-peak electricity and delivery price in Ontario
Day_{Active}	The number of active days considered for service vehicles	260 work day a year in Canada by Statistics Canada [52]
$Years$	Targeted life span of the system for the optimizer	Considering the life cycle of the battery packs and the limitation explained in Subsections 3.3.7.3 and 4.3.5, the battery pack are expected to last for almost 5 years without need for replacement due to degradation
$Battery_{Banks}$	The number of parallel set of battery banks (determined by the optimizer)	Due to available prepackaged battery packs with a nominal voltage of 12V, to match the regular vehicle's electrical system, the optimizer just determines the number of parallel battery cells in the battery pack (All set of series cells are considered predefined)
$Battery_{Cost}$	The unit price of each prepack battery bank or each series set of battery bank cells from Table 3-1	Prices of the battery pack from the Canadian distributors' websites
$Accessory_{Cost}$	Total cost of added initial parts	Estimated price for the initial parts in the low duty service vehicle RAPS, as explained in Subsection 4.3.3 and Table 4-1.
$ERROR$	Zero or a large number	Error signal included in the objective function evaluation to prevent the optimizer from choosing the impossible cases (such as demanding more power than the maximum available engine power)

4.3.5 Limitations and Constraints

There are different limitations and constraints that should be considered. These limitations can be because of mechanical and physical limitations, availability of materials, maintenance issues, cost considerations, or many other reasons. In this study, each of the optimization valuables has its own constraint:

- **Low and high-level battery SOC thresholds**

  These first two optimization variables have almost the same limitations and are related constraints. Battery prices and life cycle span are important in the total system cost. One of the most important factors that can change the battery life cycle is the battery DOD, which can be actively controlled by utilizing optimized power management control strategy logics. Depth of discharge (DOD) is the difference between 100 percent battery SOC level (full battery) and present battery SOC level. For instance, a complete discharge cycle to 0% SOC is equivalent to 100% DOD, or a 50% discharged battery (SOC equal to 50%) has DOD of 50%. The optimization boundary for the battery SOC thresholds (or DOD thresholds), particularly at the low level, should be selected accurately in order to make sure that the battery cells do not need replacement during the expected working periods of RAPS.

  The other constraint that should be considered for the low and high-level battery SOC thresholds is that there should be at least a 5 percent difference between these two battery SOC thresholds. This 5 percent difference is to avoid having the controller switch frequently between the two possible conditions (high-efficiency engine condition and regular low-efficiency engine condition), which may cause the

generator to turn on and off frequently when the battery SOC stays around the threshold values. This 5 percent difference is chosen based on a trial and error process. This logical concept is applied using the constraint vector $C(X_D)$ based on the method in [58].

- **Number of battery packs**

The first constraint in battery packs optimization is that the number of series cells is constant (different constant number for different battery models) and in the optimization process, they are not considered to hold the nominal voltage in the same range for all of the chosen battery packs.

The second constraint for the battery sizing is based on equation (3-38), as represented again by:

$$I_B = \frac{-V_{B\_OC} \pm \sqrt{{V_{B\_OC}}^2 + 4P_{B\_\text{Desired}}R_{In}}}{2R_{In}} \tag{4-10}$$

From this equation, the important constraint is that the total value of the term under the radical should be always non-negative so that the current has a real value. The values of R_{In}, and V_{B_OC} , which represent the internal resistance and the open circuit voltage of the battery, respectively, are always non-negative. However, during the discharge of the battery, the value of the battery power (P_{B_Desired}) is negative. In this condition, $4R_{In}$ should be so low such that the term ${V_{B\_OC}}^2$ will always be larger than absolute value of term $4P_{B\_\text{Desired}}R_{In}$. The value of R_{In} will be low when there are enough parallel battery packs connected. Therefore, the second constraint is the

minimum number of parallel battery cells. An error signal in the Simulink model shows this constraint. This error signal will be active in the discharge condition if the value of ${V_{B\_OC}}^2$ becomes smaller than absolute value of $4P_{B\_\mathrm{Desired}}R_{In}$. Based on the description in Subsection 4.3.4, if $ERROR$ is activated, the optimizer will not choose that solution.

The last constraint for the battery sizing relates to the output power of the ESS (total battery pack system). The battery pack should have enough parallel cells to provide the maximum demanded power of the auxiliary devices at all times. During the discharge conditions, the output voltage of battery pack decreases from the nominal voltage. In addition, as long as batteries are not at their very high and very low SOC level, it can be assumed that the discharge current and voltage can be considered constant. The constant values for the different selected battery models in this study are presented in Table 4-3. These values will change slightly based on environmental factors such as temperature; however, due to the lack of information, the reported values are based on the available discharge curves for the selected battery models from the data sheets from manufacturer or dealer websites.

For the battery packs, the maximum continuous discharge power is defined as the multiplication of the discharge voltage with the maximum continuous discharge current. This value is compared to the maximum demanded auxiliary power of 1,100 [W] (based on the industrial partner's suggested service cycle) to determine the minimum number of needed battery packs, which is an integer number, for providing the demanded auxiliary power. This "Minimum Required Battery Pack to Provide 1.1

kWh Auxiliary Power [Number]" is set as the lower bound of the optimizer for the number of parallel battery packs.

Table 4-3: Assumed output power of different chosen battery models

Battery Type	Voltage [V]	Maximum Continuous Discharge Current [A]	Maximum Continuous Discharge Power [W]	Minimum Required Battery Pack to Provide 1.1 kWh Auxiliary Power [Number]
EV12_140X DiscoverDryCell	12	105	1260	1
EV12_180X DiscoverDryCell	12	135.75	1629	1
EV12_8DA_A DiscoverDryCell	12	195	2340	1
EV12_Li_A123 ALM12V7	12.2	18.4	224.48	5
EV12_Li_A123 ANR26650	10.8	40	432	3
EV12_Li GBS_100Ah	12	300	3600	1

4.4 Case Studies

In order to show the impact of adding the regenerative braking system to the vehicle and optimizing the total system, different simulation conditions are considered to illustrate the impacts of utilizing the proposed system on fuel consumption in service vehicles. To simulate a whole working day of service vehicles, two different drive cycle are considered:

- **General Drive Cycle:** This drive cycle, as shown in Figure 4-3, is created based on three times of randomly repeating five common standard drive cycles (namely "UDDS", "FTP75", "HWFET", "NYCC", and "US06") and adding idling durations. During this 18040 seconds drive cycle, the vehicle is moved 182 Km.

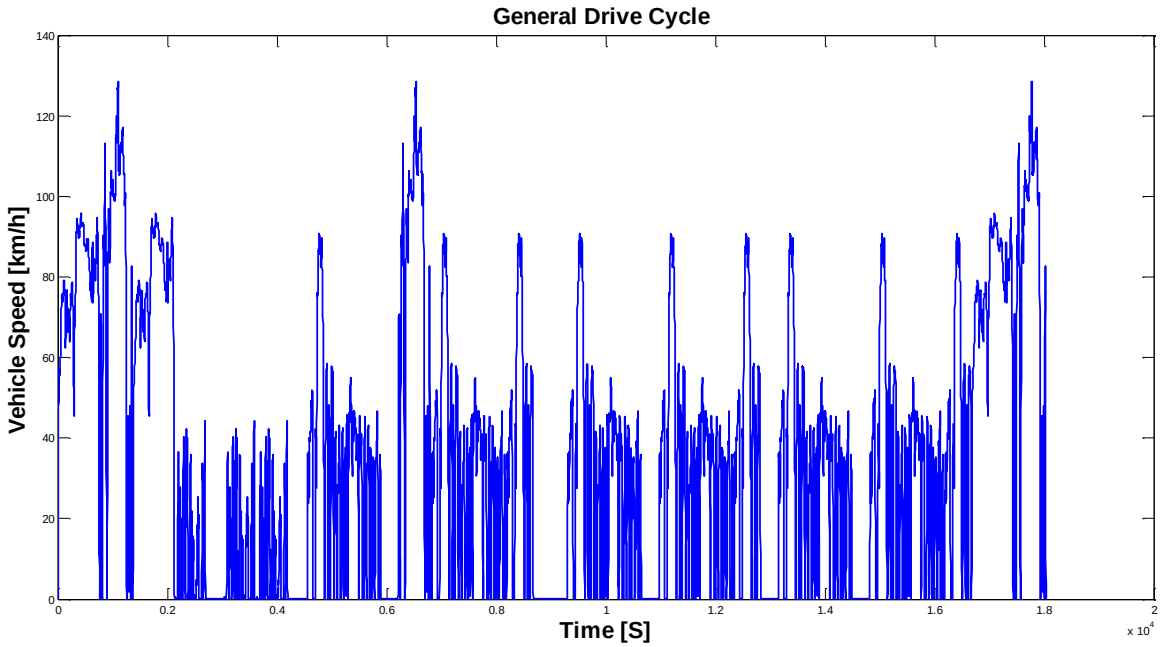

Figure 4-3: General Drive Cycle

- **Industry Partner Drive Cycle:** Based on suggestions of the project's industrial partners, a shorter drive cycle as shown in Figure 4-4 is considered. It is considered that the service vehicle has a 30-minute highway ride from the warehouse to the distributing city and then 5 unloading stops, each one for 5 minutes. Between each of these unloading stops, there will be a 15-minute city drive. The drive cycle, as shown in Figure 4-4, is mathematically modeled based on these assumptions. For the two highway rides "HWFET" and for city driving "NYCC" standard drive cycles are utilized for modeling this suggested drive cycle. During this 8323 seconds drive cycle, the vehicle is moved 91Km.

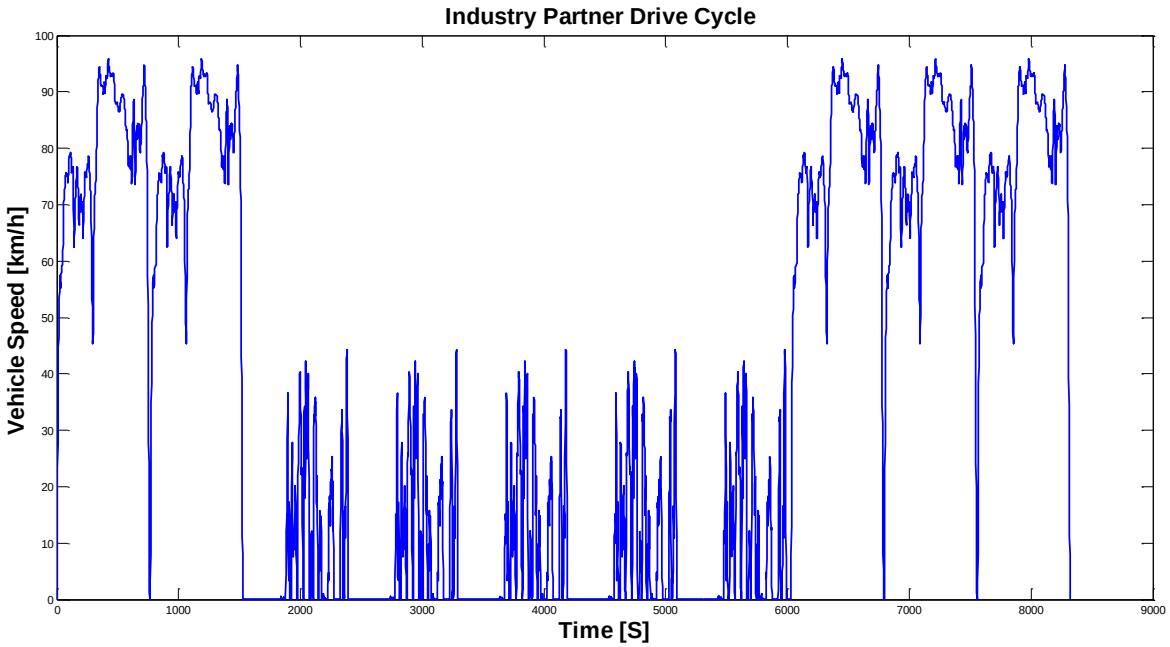

Figure 4-4: Industry Partner Drive Cycle

- **Auxiliary Load Service Cycle:** "T110D no-idler reefer" unit for the refrigerator van is considered as the auxiliary device for the targeted service vehicle. This unit has an auxiliary power load of 1.1 kW. Based on the suggestions of the project's industrial partners, an on-off auxiliary load of 1100 [Watt] (as shown in Figure 4-5) is applied as the demanded electrical load for the auxiliary devices.

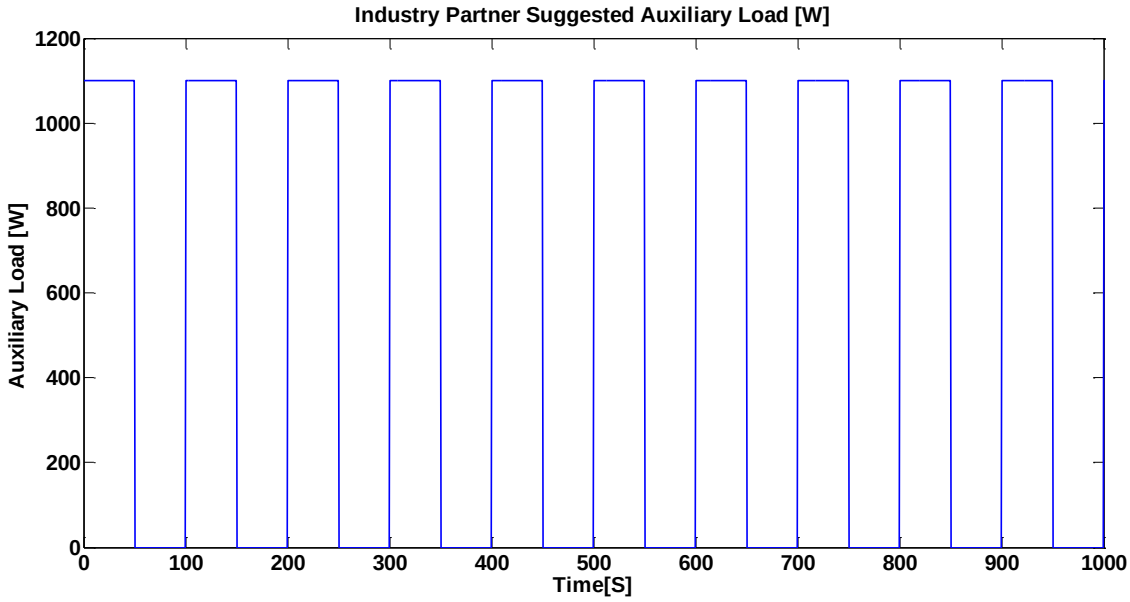

Figure 4-5: Service Vehicles Auxiliary Load Suggested by Industry Partner

4.4.1 Case Study: GMC Savana 2500

The "GMC Savana", a common target vehicle in the food delivery service, is selected for the simulation study. The specifications of this vehicle are presented in Table 4-4. In order to show the impact of adding the regenerative braking system to the vehicle and optimizing the total system, design optimization process is performed for this vehicle. There is a tradeoff between the number of the battery packs and the total system cost and fuel consumption since added battery pack will increase the total weight of the system.

Two optimization methods (genetic algorithm (GA) and simulated annealing (SA)) are used to optimize the number of battery packs, the low and high level battery SOC thresholds (as defined in the first part of Chapter 4). The results of these optimization procedures for the six chosen battery models and two drive cycles are shown in Table 4-5 and Table 4-6.

In the optimization procedures simulation models of the conventional vehicle (vehicle model with the auxiliary power which is directly loaded to the engine) and the RAPS vehicle are run against both drive cycles. In the conventional vehicle model, when the auxiliary power is on, the amount of demanded auxiliary torque in each engine speed is calculated. This extra torque is added to the regular torque of a conventional vehicle during driving or idling. Conversely, in the RAPS vehicle model, the demanded auxiliary power is provided by the stored energy of the added battery packs, which are charged using regenerative braking energy (wasted energy in the conventional vehicles), plug-in electricity energy (cheaper than the fuel used in the engine to provide the same amount of energy), and directly from engine in high engine efficiency conditions. It should be mentioned that the main objective of the optimization is to minimize the total cost which consists of initial system cost and energy consumption cost during five-year interval.

Table 4-4: GMC Savana 2500 Specifications

Model	GMC Savana 2500 (Gasoline)
Engine capacity [L]	4.8
Transmission	6 Gears Automatic
Total vehicle mass without cargo [Kg]	2415
Cargo mass [Kg]	300
Tire efficient radius [Cm]	36.76
Tire mass [Kg]	22
Air density [kg/m^3]	1.2
Vehicle frontal area [m^2]	4.16
Drag coefficient of vehicle	0.32
Rolling resistance coefficient	0.01

Table 4-5: Optimization results for GMC Savana during general drive cycle

Battery Model		EV12_140X Discover DryCell		EV12_180X Discover DryCell		EV12_8DA_A Discover DryCell		EV12_Li_A123 ALM12V7		EV12_Li_A123 ANR26650		EV12_Li GBS_100Ah	
Optimization Method		GA	SA	GA	SA	GA	SA	GA	SA	GA	SA	GA	SA
Low Level Battery SOC [%]		75.29	70	75.28	70.01	72.14	70.43	37.58	30.97	33	30.02	33.03	30.67
High Level Battery SOC [%]		80.64	75.02	80.66	75.09	77.75	75.53	52.82	46.15	48.11	45.09	85.14	83.02
Number of Battery Packs		3	3	2	2	2	2	18	17	30	28	1	1
Added System Cost	Total Initialization Cost [$]	3661	3661	3322	3322	3672	3672	6142	6001	6041	5975	6109	6109
	Total Plug-in Electricity Cost [$]	210.4	268.63	180.81	230.82	305.08	315.15	120.36	127.56	112.21	109.93	538.22	562.94
	Total Added System Cost [$]	3871.4	3929.6	3502.8	3552.8	3977.1	3987.2	6262.4	6128.6	6153.2	6084.9	6647.2	6671.9
Fuel Saving [$]	Conventional Vehicle Fuel Cost [$]	60467	60467	60467	60467	60467	60467	60467	60467	60467	60467	60467	60467
	Optimized Vehicle Fuel Cost [$]	54918	54119	55196	54667	53928	53884	55547	55534	56982	56485	52989	52989
	Total Fuel Saving in Five Years [$]	5549	6348	5271	5800	6539	6583	4920	4933	3485	3982	7478	7478
Total Saving by Utilizing RAPS [$]		1677.6	2418.4	1768.2	2247.2	2561.9	2595.9	-1342.4	-1195.6	-2668.2	-2102.9	830.78	806.06
Investment Returning Time [Year]		3.2988	2.8836	3.1512	2.8638	2.8078	2.789	6.2419	6.0825	8.6671	7.5025	4.0846	4.0846

Table 4-6: Optimization results for GMC Savana during industry partner drive cycle

Battery Model		EV12_140X Discover DryCell		EV12_180X Discover DryCell		EV12_8DA_A Discover DryCell		EV12_Li_A123 ALM12V7		EV12_Li_A123 ANR26650		EV12_Li GBS_100Ah	
Optimization Method		GA	SA	GA	SA	GA	SA	GA	SA	GA	SA	GA	SA
Low Level Battery SOC [%]		70.46	70	70.88	70	70.82	70	38.72	30.01	30.07	30	31.56	35.45
High Level Battery SOC [%]		85.72	84.89	88.16	87.14	78.95	75.14	46.2	45.05	89.92	84.39	86.81	84.89
Number of Battery Packs		1	1	1	1	1	1	9	8	10	11	1	1
Added System Cost	Total Initialization Cost [$]	2353.7	2353.7	2461.1	2461.1	2636.2	2636.2	4671.3	4530	3772.9	3810.2	4027.2	4027.2
	Total Plug-in Electricity Cost [$]	89.057	90.744	113.24	117.41	163.47	169.06	60.35	62.09	155.7	171.5	192.93	153.49
	Total Added System Cost [$]	2442.8	2444.4	2574.3	2578.5	2799.7	2805.3	4731.7	4592.1	3928.6	3981.7	4220.1	4180.7
Fuel Saving [$]	Conventional Vehicle Fuel Cost [$]	30250	30250	30250	30250	30250	30250	30250	30250	30250	30250	30250	30250
	Optimized Vehicle Fuel Cost [$]	25502	25444	24842	24763	24169	24145	26246	26339	25856	25953	23906	23784
	Total Fuel Saving in Five Years [$]	4748	4806	5408	5487	6081	6105	4004	3911	4394	4297	6344	6466
Total Saving by Utilizing RAPS [$]		2305.2	2361.6	2833.7	2908.5	3281.3	3299.7	-727.65	-681.09	465.4	315.3	2123.9	2285.3
Investment Returning Time [Year]		2.4786	2.4487	2.2754	2.2427	2.1676	2.159	5.8333	5.7914	4.2932	4.4336	3.174	3.1141

According to Table 4-5 and Table 4-6, Generic Algorithm (GA) and Simulated Annealing (SA) optimization methods have close results. Optimal solution (lowest total system cost or highest saving) is happening when “EV12_8DA_A Discover Dry Cell” battery packs are used. From the optimization results, it can be seen that for the shorter drive cycle (industry partner drive cycle) generally fewer battery packs are needed in the EES. Since in this drive cycle the operating time of service vehicle is lower than the general drive cycle; EES with less electrical capacity can provide the optimal system cost. However, for the longer drive cycle (with more fuel consumption) decrease in the total fuel consumption and total system cost compensates the increase of cost due to bigger EES.

In Table 4-5 and Table 4-6, the total initialisation cost of the RAPS (consisted of the battery pack and initial parts) are shown. Moreover, fuel consumption of the conventional service vehicle and the vehicle utilizing RAPS are compared. The saving in the fuel consumption cost is the main benefit of RAPS which compensate the initial cost of the system and results in the total saving. The value of fuel cost saving and total saving using RAPS are presented in “Total Fuel Saving in Five Years [$]” and “Total Saving by Utilizing RAPS [$]” rows respectively.

The expected return time for the initial investment is shown in the last row. For the optimal RAPS, the initial investment will be returned after 2 to 3 years, which is half the expected lifetime of the batteries. Comparing results from Table 4-5 and Table 4-6, it can be seen that the expected return time for the initial investment is less for the industry partner drive cycle. Which means utilizing RAPS for that drive cycle provides better investment return. This can be due to two reasons: 1) The percentage of idling time to the total drive

cycle time is higher in the industry partner drive cycle, therefore, there is more need and benefit for RAPS in industry partner drive cycle. 2) The percentage of city driving time to highway driving time is higher in the industry partner drive cycle. This causes more stop (braking) and go during industry partner drive cycle which benefits the regenerative braking systems like RAPS.

DOD feature of lithium-based batteries and their low weight comparing to the same capacity dry-cell batteries, makes the lithium-based batteries an interesting choice; however, for this case study that the number of battery packs are a few, the higher initial cost of lithium-based batteries (especially "EV12_Li_A123 ALM12V7" and "EV12_Li_A123 ANR26650") increase the total system cost that the benefits of lithium-based batteries cannot compensate the extra costs. This is the reason for the negative value in the "Total Saving by Utilizing RAPS [$]" row in Table 4-5 and Table 4-6.

Based on optimization results, simulation models of the conventional vehicle (vehicle model with auxiliary power which is directly loaded to the engine) and the optimal RAPS vehicle (best design from optimization) are run against both drive cycles, and the results are shown in Table 4-7.

Table 4-7: Vehicle Models Simulation Results

Model	Conventional Vehicle Model		Optimal RAPS Vehicle Model	
	Industry Partner Drive Cycle	General Drive Cycle	Industry Partner Drive Cycle	General Drive Cycle
Fuel Consumption: [L] gasoline per day (Drive Cycle)	15.51	31.01	13.15	27.63
Fuel Consumption: [L] gasoline for 5 years	20167	40313	17095	35919

Based on the results from Table 4-7, it is clear that utilizing RAPS will decrease fuel consumption remarkably (15% and 11% total fuel saving for “Industry Partner” and “General” drive cycles respectively). During the 5 years expected life cycle of RAPS, 3072 [L] and 4394[L] gasoline will be saved when driving with the “Industry Partner” drive cycle or the “General” drive cycle, respectively.

Chapter 5

Experimental Validation

Experimental results are essential to proving the effectiveness of the proposed RAPS and validating the simulation results. Before prototyping the RAPS on a real vehicle, the design should be tested by laboratory facilities. Hardware-in-the-loop (HIL) test stand has been utilized for the laboratory evaluation in order to validate component models, characterize the RAPS components, and implement and modify the controller strategies. A prototype model of RAPS (containing the generator, battery, auxiliary load, and control system) is developed. Characterization and model modification-verification of RAPS components are performed utilizing this setup. For the power management control strategy, controllers are implemented in the RAPS prototype system. Utilizing this prototype, different scenarios are simulated to investigate the real world limitations, to modify the optimization constraints, the components' model, and to implement and develop the control strategies in the experimental conditions. This evaluation will help fine-tune the prototype for installation on a real service vehicle.

5.1 Experimental Setup: Hardware-In-the-Loop (HIL)

In order to simulate the real world conditions for laboratory evaluation, a RAPS laboratory prototype is fabricated. Different parts of this prototype and their places in the system are explained in Figure 5-1 and Figure 5-2. The schematic installation connection for the low power demand (serpentine belt) and high power demand (aperture PTO) configurations are also shown in Figure 5-3 and Figure 5-4, respectively. This prototype is a combination of

dynamometers (simulating the mechanical part of the real vehicle), RAPS components (generator and battery for low and high power demands, PTO for high power demands), and load simulator (simulating expected electrical load of auxiliary devices).

Based on the available parts in the market and optimization results, suitable electrical parts (Discover dry-cell 8DA_A deep dry lead-acid battery and high output alternator) are purchased and installed in order to develop a regenerative braking system that maximizes power extraction.

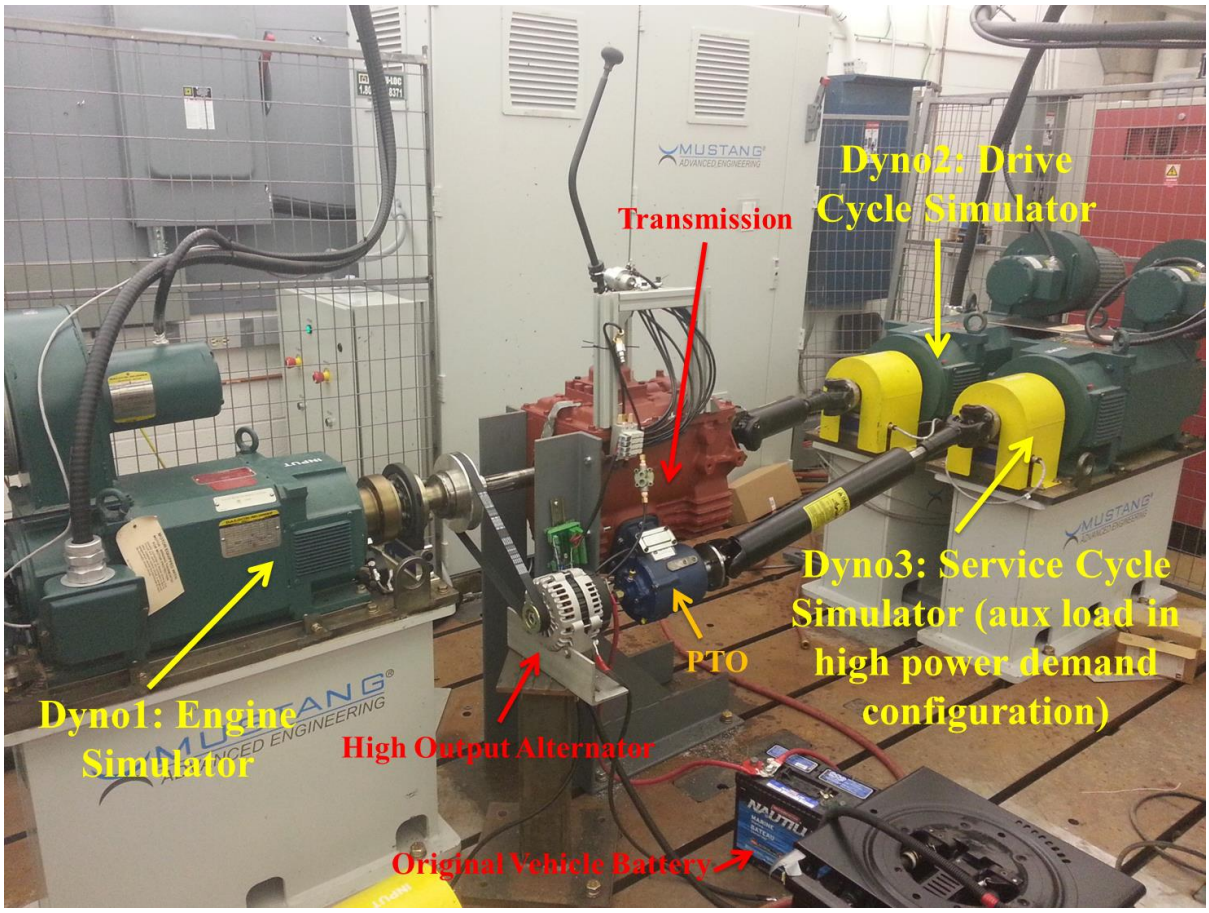

Figure 5-1: Hardware-in-the-loop facilities installed in the Mechatronic Vehicle Systems laboratory

For simulation of the mechanical parts of the targeted vehicle, a “Mustang Dynamometer”, as shown in Figure 5-1 and Figure 5-5, has been utilized. In this test stand, the input dyno (Dyno1), which acts as the vehicle main engine, is connected to two other dynos through the transmission and the PTO. The vehicle’s traction force simulator dyno (Dyno2), which act as the wheels traction, braking torques, and drive cycle simulator, is connected to the transmission output shaft. This dyno simulates the impact of the vehicle’s traction force at the transmission output as the resistance (negative) torque opposed to the input dyno’s torque (positive). The auxiliary load simulator dyno (Dyno3), which acts as the service cycle simulator, is connected to the PTO output shaft. This dyno simulates the impact of the auxiliary load as a resistance (negative) torque in the high power demand configuration. By programming these dynos, the RAPS can be tested against different conditions in a controlled environment.

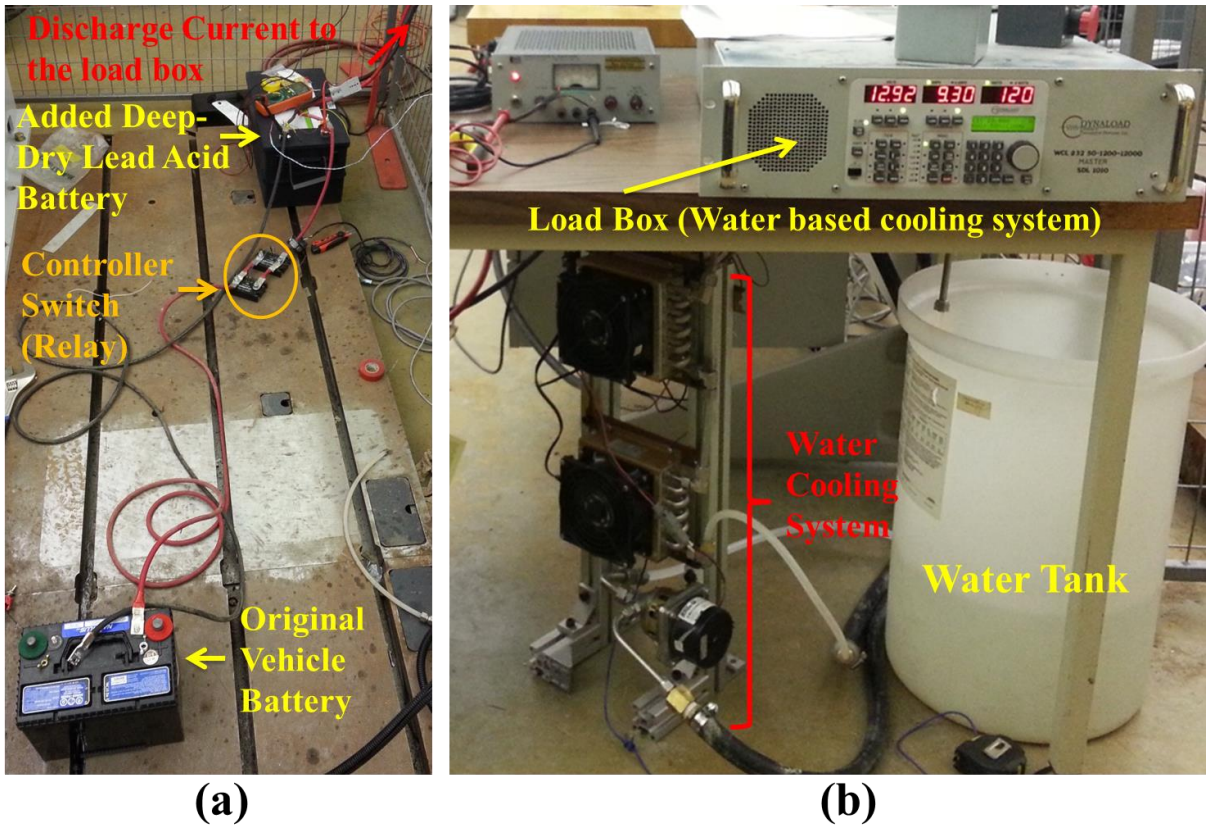

Figure 5-2: a) Electrical part of RAPS prototype model; b) Load box (Auxiliary load simulator in low power demand configuration)

For the low power demand (serpentine belt) configuration, there is no need for the PTO, and the dyno 3 is disconnected from the system. Since in this condition the amount of demand power is low, there is no need for a special generator, and a regular high output alternator is utilized to create the auxiliary load impact on the powertrain. As shown in Figure 5-6, the alternator is connected to the shaft between dyno1 and the transmission through a set of pulleys and a serpentine belt. This installation has a similar shape to a real serpentine belt configuration in service vehicles. A high output alternator for the "GMC Savan 2500", one of the targeted vehicles for RAPS design, charges the EES and provides the demanded power by the load box.

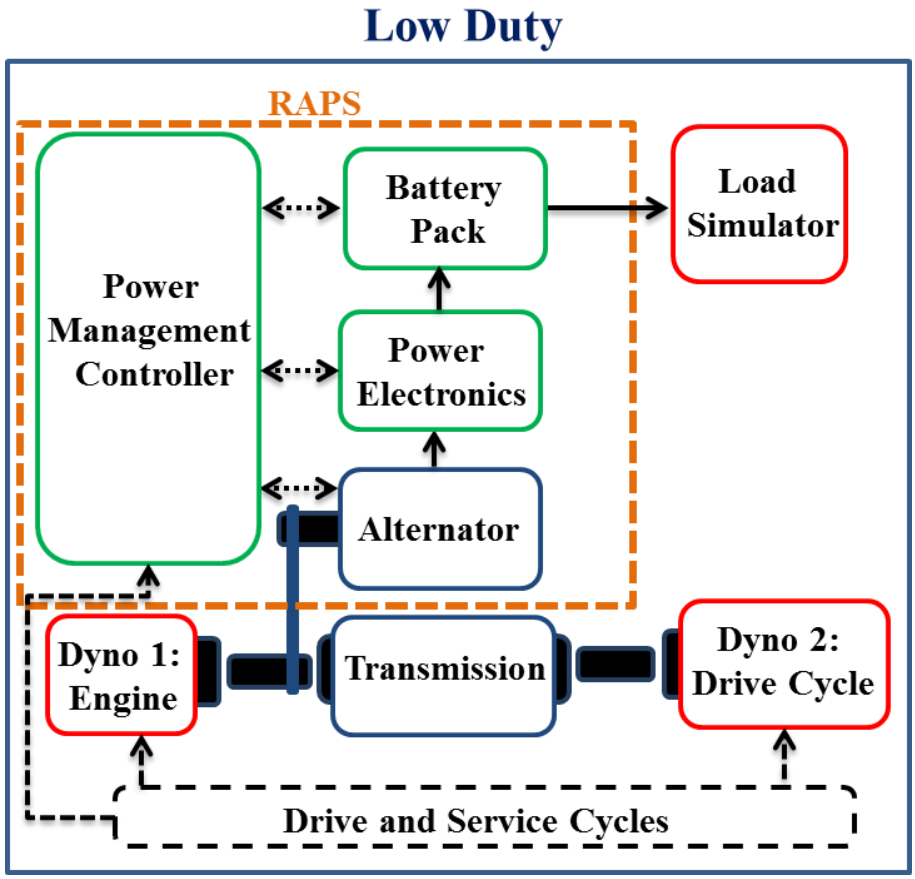

Figure 5-3: Schematic installation connection for low power demand (serpentine belt) configuration

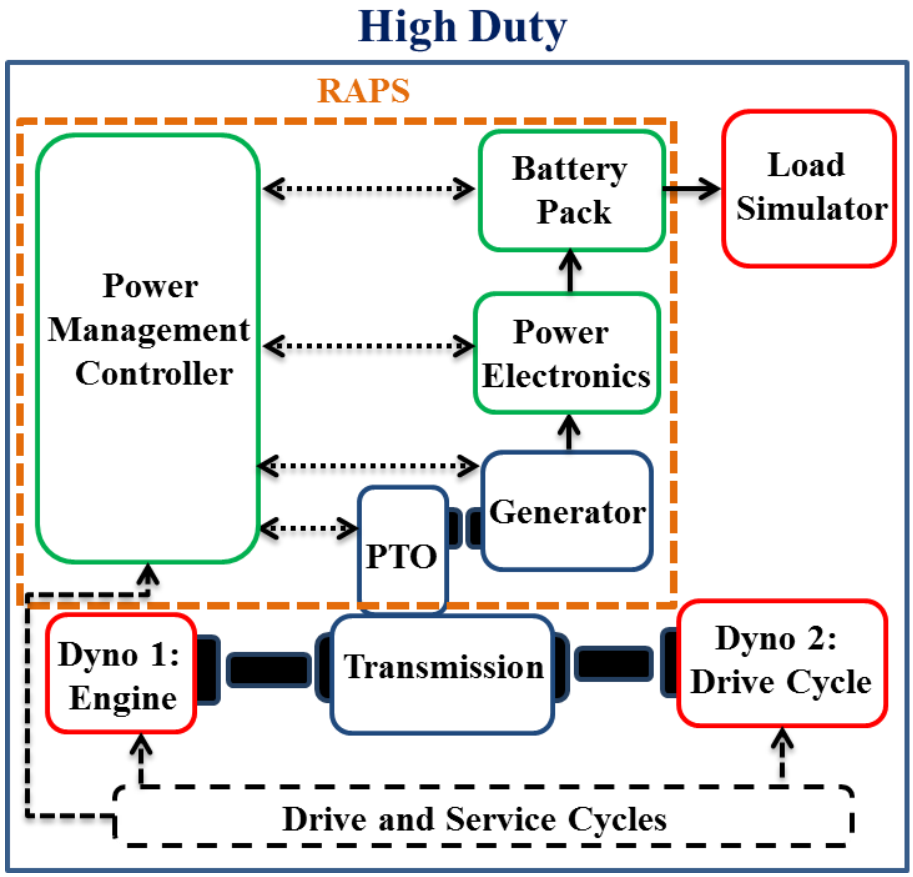

Figure 5-4: Schematic installation connection for high power demand (aperture PTO) configuration

Figure 5-5: Conceptual picture of "Mustang Dynamometer" (HIL test stand) [59]

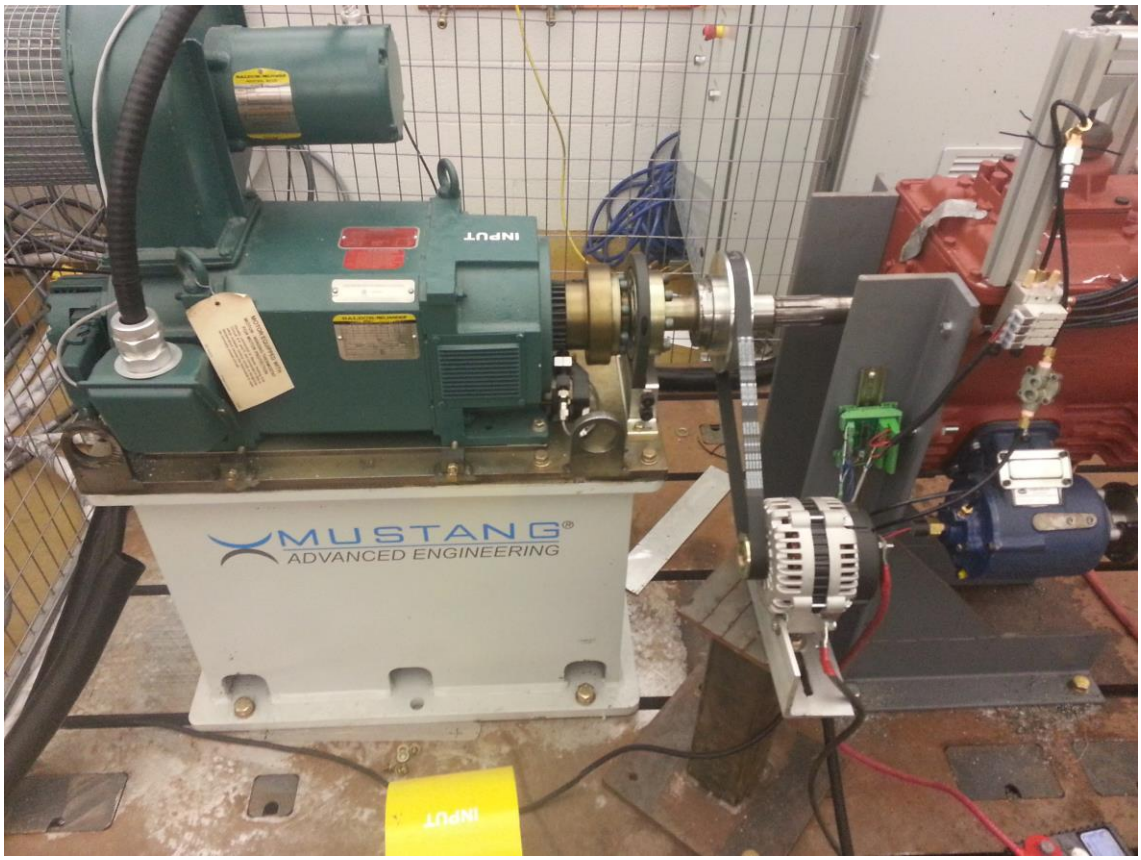

Figure 5-6: Alternator connection to the dynamometer

5.2 Experiments Procedure

Considering the developed prototype RAPS and HIL facilities, different experiments were designed and performed to characterize the RAPS components, validate and modify the components' model, and implement and tune the controllers. These experimental procedures are explained in this section.

5.2.1 Alternator-Generator Characterization Experiments Procedure

Due to the fact that in this study, the power consumption of the vehicle and the regenerative power is of interest, the Alternator-Generator, which is the main power source for charging the EES (the other power source is plug-in during the night), should be accurately modeled and characterized. Two sets of tests are designed and performed to create the "Maximum current versus alternator angular velocity" and "Efficiency map" curves of the alternator.

The prototype RAPS alternator is an internally-regulated, self-exciting (one-wire) alternator. In order to make it work, there is a need for a minimum alternator angular velocity and a very low starting electrical energy just during starting process. To find the "Maximum current versus alternator angular velocity" curve, a different constant angular velocity is provided by dyno1 through the system shown in Figure 5-6. The alternator is loaded by a systematically increasing load (Figure 5-7) that is demanded by the auxiliary load simulator (Figure 5-2 b) until it reaches the alternator load limit at that angular velocity. Repeating this process at a different constant angular velocity in the working range of the alternator determines the maximum possible current load value in each angular. Plotting the resulted maximum possible current load points in each angular velocity versus alternator angular velocity will create the "Maximum current versus alternator angular velocity" curve

(Figure 5-8). This curve will rule the range of current and angular velocity for the "Efficiency map" experiment, which is the main purpose of the alternator characterization process.

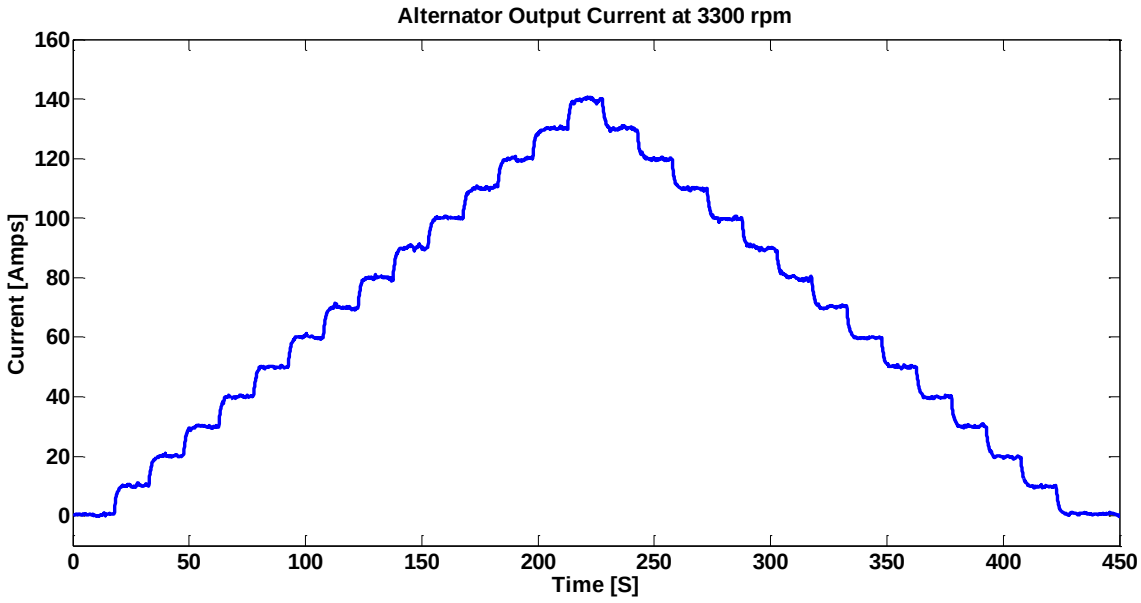

Figure 5-7: Systematically increasing loading of alternator during maximum current determination at 3300 rpm

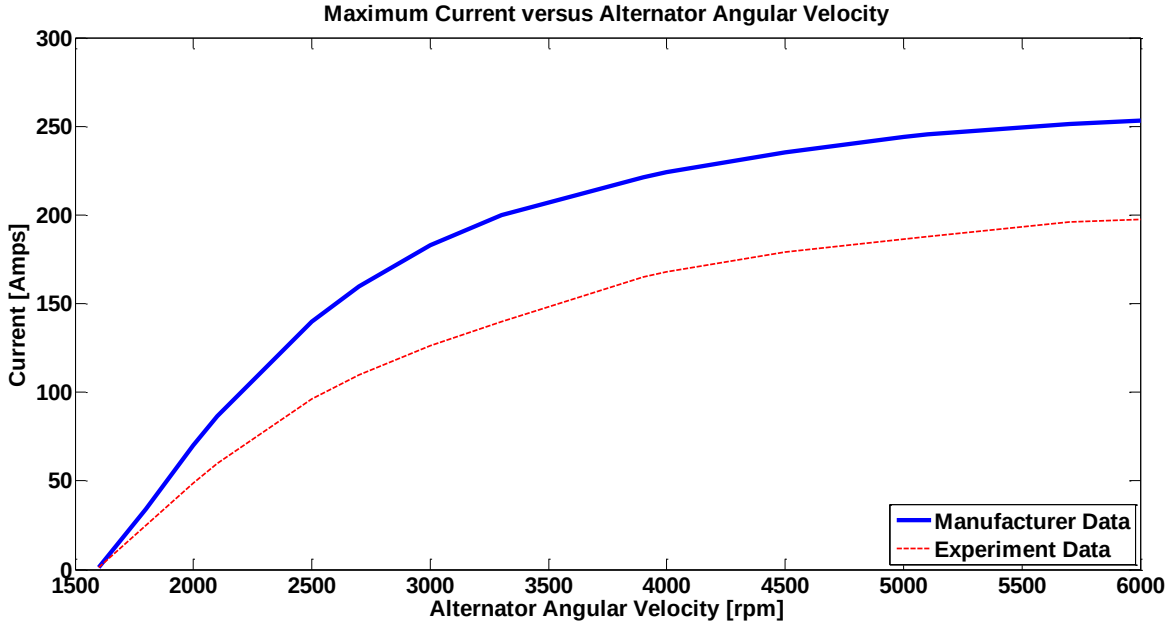

Figure 5-8: "Maximum current versus alternator angular velocity" curve

From Figure 5-8, it can be seen that due to limitations of the prototype, such as the serpentine belt tension, the maximum current at each angular velocity is lower than the reported data by the manufacturer; however, both plots have the same shape and the prototype alternator fulfills the maximum desired current conditions.

In order to create the "Efficiency map" curve, a similar systematical alternator load increasing experiment as shown in Figure 5-7 is performed. In each angular velocity (ω_G), values of input torque (T_G), alternator output current (I_G), and voltage (V_G) are recorded. By rearranging equation (3-15), the alternator efficiency can be determined as:

$$\eta_G = \frac{Output\ Power}{Input\ Power} = \frac{I_G V_G}{T_G \omega_G} \tag{5-1}$$

Repeating this process with different constant angular velocity conditions, the alternator efficiency in different sets of angular velocity and torque are determined. Figure 5-9 shows the alternator "Efficiency map" curve indexed by the input torque and angular velocity to the alternator.

From Figure 5-9, it is clear that by increasing the alternator input angular velocity, the alternator efficiency increases. For alternator speeds lower than 1800 rpm (engine speed lower than idling at about 600 rpm), the alternator will not create any current and the efficiency is zero. By increasing the alternator speed to 6000 rpm, the alternator will be saturated, and efficiency reaches the maximum value of about 70%.

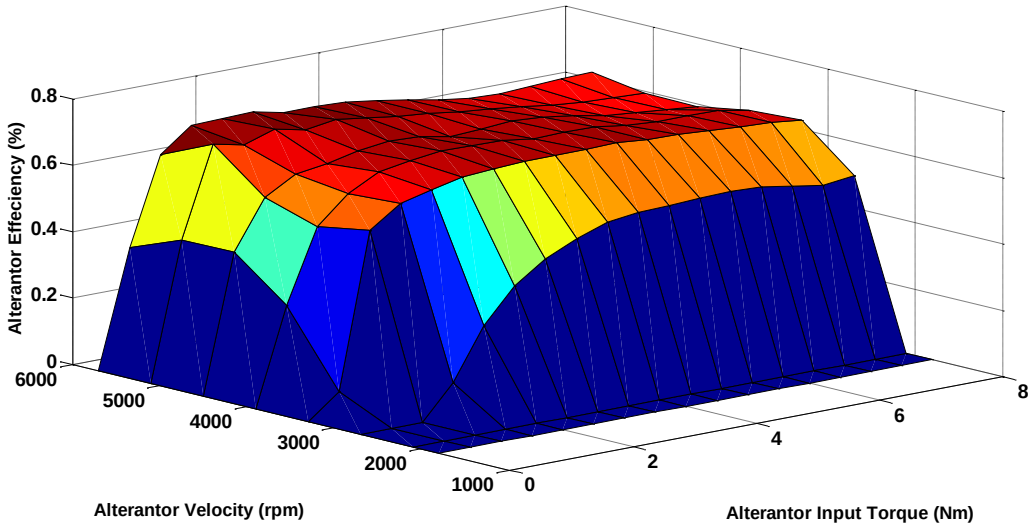

Figure 5-9: Alternator "Efficiency map"

5.2.2 RAPS Total Model Validation Experiment Procedure

For the model validation test, the setup shown in Figure 5-7 is used. Based on the limitations of the facilities, it is considered that the angular velocity of each dynamometer should not exceed 2000 [rpm]. The experimental drive cycle, as shown in Figure 5-10, is created based on repeating the "UDDS" standard drive cycle [60], to model the city driving of service vehicles, and adding idling durations, to model the loading and unloading stops. This drive cycle is used to calculate the vehicle's traction force impact at the transmission output shaft as the resistance torque. This torque is simulated in the system utilizing Dyno2. Also, the engine output angular velocity based on the experimental drive cycle is simulated in the system through Dyno1. The Dyno1 angular velocity is recorded during the experiment, as shown in Figure 5-11, to ensure its values meet the limitations of the facilities.

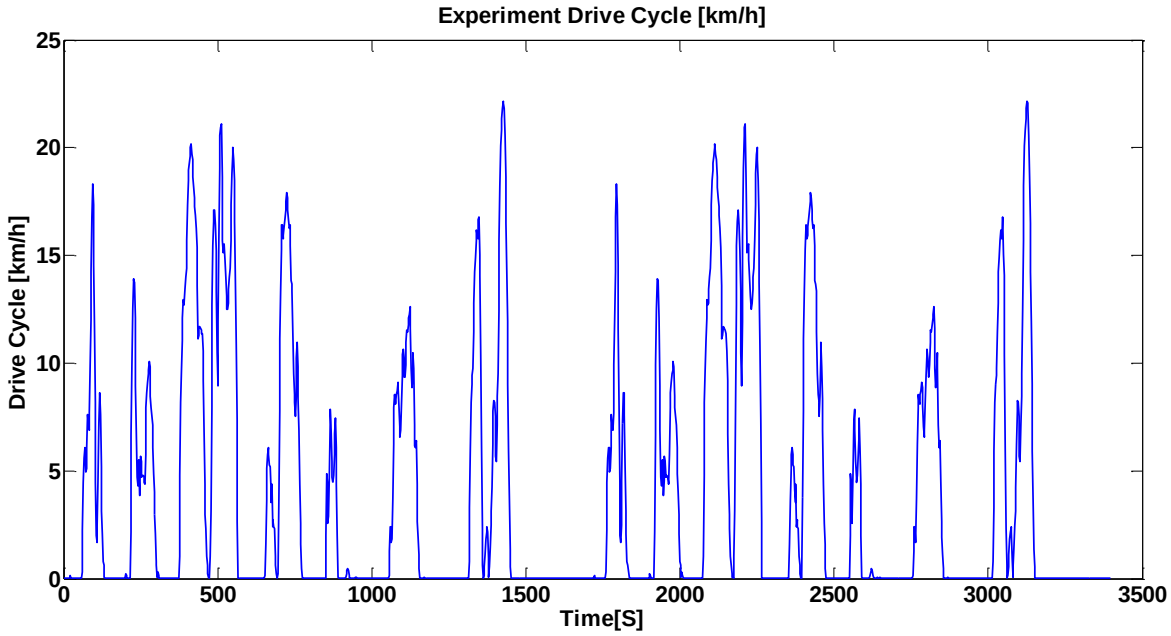

Figure 5-10: Experiment drive cycle

Due to the fact that in this study, the power consumption and power change in the real service vehicle are the main interest, the changes of the EES energy (battery SOC in this case) will be the main output of the system and present the system condition and state. As a result, during the development of the prototyped RAPS, a battery pack has been utilized (Discover EV 8DA_A deep dry lead-acid battery), and a high output alternator (GMC Savan 2500 high output alternator manufactured by Waiglobal) that is suitable for the service vehicle size suggested by our industrial partner has also been utilized. In addition, based on the industrial partner's suggestions, an on-off auxiliary load of 1100 [Watt] is applied as the demanded electrical load through the auxiliary load simulator (Figure 5-2b).

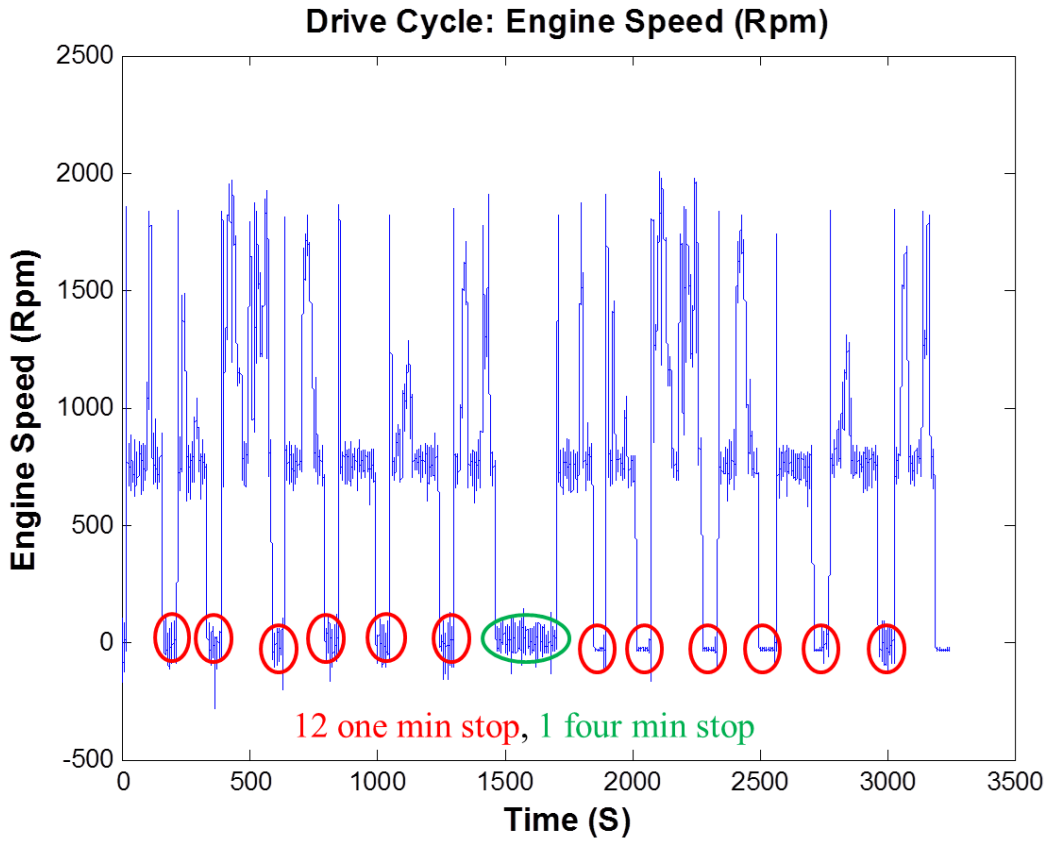

Figure 5-11: Dyno1 (Engine simulator) angular velocity

In the validation experiment, dyno1 (which represents engine in service vehicles) produces the mechanical power (based on the experiment drive cycle) as the input energy to the system. The auxiliary load simulator extracts the electrical energy from the system as the output energy. RAPS components act as the intermediate parts, which provide the auxiliary device power by utilizing the stored energy in the battery pack and the alternator charging power. In order to verify the presented modeling approach and establish its composability features, changes in the experimental battery SOC (the main output of the system) should match the battery SOC changes from the RAPS simulation model when the same drive cycle is used as the system input for both experiment and simulation. The RAPS simulation model

consisted of the RAPS components model composed together to study the features of the proposed modeling approach. This comparison is illustrated in Figure 5-12.

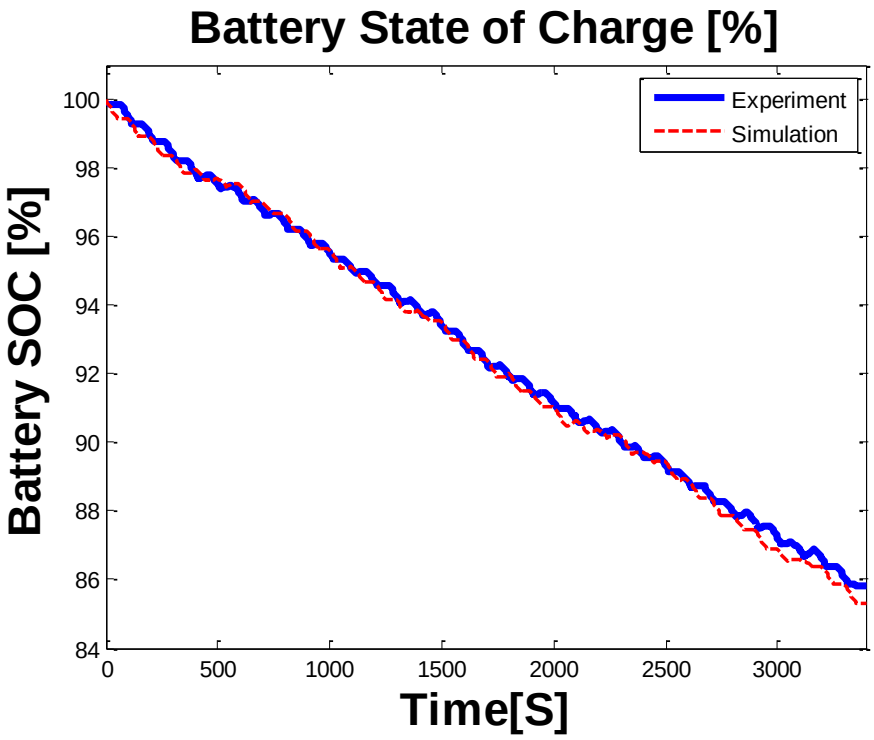

Figure 5-12: Battery SOC changes from RAPS model and RAPS prototype experiment

From Figure 5-12, it can be seen that the RAPS simulation model result mostly follows the experimental result. There are a few differences between the two plots especially at the beginning and at the end of the test. Also, although both graphs have the same pattern, there are magnitude differences at some points. These can be due to the impact of resistance forces, inertia effects, and other vehicle dynamics that have been set aside for simplification purposes of the backward-looking modeling approach. There is a close match between the overall power change in the experimental and simulation model results, which shows the practical use of backward-looking modeling approach for anti-idling system modeling in service vehicles.

Chapter 6

Concluding Remarks and Future Work

In this study, a regenerative auxiliary power system (RAPS) was proposed to prevent the idling in service vehicles. The RAPS employs waste energy during braking and provides the demanded auxiliary power for the A/C-R service vehicles. In these vehicles usually 15 to 25 percent of engine fuel consumption goes to auxiliary devices; hence, an anti-idling solution has a significant impact on the fuel consumption, air pollution and operation cost. This solution decreases fuel consumption without a large increase in the total system weight and initial cost due to a minimal amount of modification of the existing system.

Potential configurations of the RAPS and different options for integration with the vehicle powertrains were studied. Limitations of each configuration and required components that could be used to extract mechanical power for the generator in each configuration were investigated.

A library for common components' model used in service vehicles was developed. These components' models are generic, modular, and flexible with scalability and composability features. This system model can be easily modified for different vehicles. It is independent of the component size and can be scaled based on a simple scalar parameter such as displacement or power rating. Also, the system components' model can easily compose to the other related parts. These features make the model suitable for optimization process to find the optimum component size and proper charging strategy. The resulted algorithm can be utilized for design of varieties of anti-idling systems for different vehicles and applications.

Impacts of utilizing an optimized RAPS on the anti-idling and fuel consumption of a sample service vehicle ("GMC Savana 2500") were reviewed as a case study. A multi-disciplinary design optimization approach was applied utilizing two different optimization methods, Genetic Algorithms (GA) and Simulating Annealing (SA), to find the optimal component size and power management control logic simultaneously. Different lead-acid and lithium-based battery packs with their limitations and constraints were considered in order to make the results more accurate. The main objective of the optimization was to minimize the total cost which included the initial system cost and energy consumption cost during five-year interval. Therefore, a financial based objective function was developed. The impacts of different drive cycles on the optimization results were also disscussed. It was shown that by utilizing the optimal RAPS total fuel consumption of the service vehicle in the case study, decreased between 10 to 15 percent based on the drive cycle. Also, the expected return time for the initial investment was estimated about 2 to 2.5 years, which is half the expected lifetime of the batteries.

A prototype model of RAPS (containing generator, battery, auxiliary load, and control system) was developed based on the case study optimal solution. Hardware-in-the-loop (HIL) was utilized to simulate vehicle powertrain components. The RAPS prototype and HIL were used for laboratory evaluation of the proposed RAPS. It was shown, that there was a close match between the experimental and simulation results.

6.1 Thesis Contributions

To achieve the objective of this research, the following tasks have been conducted:

- A generic, modular, and flexible vehicle's powertrain and RAPS components model is created using a scalable perspective to make it easy for use in different configurations and different vehicle sizes. This model is used for energy efficiency consumptions of the vehicle system in order to optimize the total cost of the system during the expected life cycle of the system.
- An algorithm platform is created to optimize the system sizing and power management logic control by utilizing multi-disciplinary design optimization method. A cost based objective function is developed to consider different component and consumption costs. Different limitations and constraints of utilizing the ESS is considered in the optimization in order to make the results more accurate.
- A survey and comparison of different battery types and optimization algorithms are performed in order to make the best selection for the case studies and different configurations (low and high power demand service vehicles). The advantages and disadvantages of different optimization algorithms for the purpose of this study are discussed. It was found that optimization methods such as a genetic algorithm or simulating annealing can be capable of finding the optimal solution.
- A prototype model of RAPS (containing generator, battery, auxiliary load, and control system) is developed for the laboratory evaluation in order to validate the components' model, characterize the RAPS components, and modify controller strategies. Characterization and model modification-verification of RAPS components is performed by utilizing this setup. By utilizing this prototype, different scenarios are simulated to investigate the real world limitations of the proposed RAPS, implement and modify the

controllers, tune the optimization constraints, and validate the components' model. This evaluation will help fine-tune the prototypes for installation on a real service vehicle.

6.2 Future Work

6.2.1 Modifying the Optimization Process

One future work may focus on increasing the optimization variables in order to have more options of decreasing the fuel consumption and acquire more options of system sizing. This can be considered by optimizing the generator and the PTO (power take off in heavy-duty vehicles) size and prices.

A decrease in optimization time is also desired. A huge portion of optimization time is spent during Simulink model run-times. A feature-based optimization can decrease the optimization time by avoiding the repetition of Simulink vehicle model simulations. A statistical map of velocity and acceleration information of a drive cycle can be developed. A 3D histogram of the drive cycle will help determine the range of velocity and acceleration values. The Simulink vehicle model should be constructed using different combinations of velocity and acceleration in order to create an energy map of the velocity and acceleration range of the 3D histogram. This energy map can be used to determine the energy consumption of the drive cycle. Hence, during each optimization iteration, only the drive cycle energy consumption calculation is repeated. The Simulink vehicle model simulation will be needed only when a new energy map need be created. For further details regarding this process references such as [61] and [37] are suggested.

6.2.2 Considering Service Vehicle Cargo Weight Cost

It is very important for fleet companies to be able to move more produces and increase the load of the vehicles. These companies demand an increased cargo weight, which increases their financial benefits. The extra weight of the added parts of the hybrid or RAPS will decrease their interest in those systems. Although, a benefit of the proposed RAPS is that it weighs less than the hybrid system; the change (decrease) in the cargo weight and load capacity of the service vehicle should be considered in the financial analysis. It is expected to find an average estimation benefit price for the unit cargo weight of targeted service vehicles and add a term to the objective function concerning the value that will be lost due to a decrease in cargo capacity of the vehicle. It should be mentioned that this value is remarkable depending on the availability of the price estimation for the benefits of cargo shipment based on weight.

6.2.3 Different EES and Battery Pack Degradation Function

Different EES packs consist of various types of rechargeable batteries or supercapacitors that can be utilized and studied in order to investigate their impact on the total simple cost and complexity of the control logic. Battery degradation and other changeable features of the EES can be included in the optimization process. This could benefit the overall system cost by estimating a longer life cycle or considering a higher DOD threshold, which means more usage of battery capacity. For example, the degradation coefficient α can be considered in the cost of the battery. This coefficient can be estimated as:

$$\alpha = e^{\frac{DOD}{K_D}} \tag{6-1}$$

in which DOD is the depth of discharge threshold of the battery, and K_D is the degradation factor, which is a scaling variable to define the battery degradation function over the period of operation. This factor can be estimated for each EES pack based on the manufacture's data sheet or discharge curves.

6.2.4 Field Testing Prototype

As the final step for industrialization of this research, prototyping the designed RAPS in a real service vehicle and testing and evaluation in different operational conditions is suggested. This prototype should meet safety and operational conditions and the results will play an important role in final modifications to the overall system development.

Bibliography

[1] H. A. Brodrick, C., Sperling, D., Dwyer, "Will Diesel Engines Make a Comeback? Energy Efficient and Now Less Dirty," *Consumers' Research Magazine*, pp. 18–21, 2002.

[2] T. J. Hendricks, "Optimization of Vehicle Air Conditioning Systems Using Transient Air Conditioning Performance Analysis," *SAE Tech. Pap.*, May 2001.

[3] R. Farrington and J. Rugh, "Impact of Vehicle Air- Conditioning on Fuel Economy , Tailpipe Emissions , and Electric Vehicle Range Preprint," in *Earth Technologies Forum*, 2000.

[4] J. Penney, "Situational Analysis : The Status of Anti-idling By-laws in Canada," 2005.

[5] Medical Officer of Health, "Improving Toronto ' s Idling Control Bylaw," 2010.

[6] H. C. Frey and P.-Y. Kuo, "Best Practices Guidebook for Greenhouse Gas Reductions in Freight Transportation," Raleigh, 2007.

[7] M. A. Tunnell and V. Dick, "Idle Reduction Technology : Fleet Preferences Survey," Alexandria, 2006.

[8] G. Gereffi and K. Dubay, "Auxiliary Power Units: Reducing Carbon Emissions by Eliminating Idling in Heavy-Duty Trucks," 2008.

[9] P. Y. KUO, "Evaluation of Freight Truck Anti-Idling Strategies for Reduction of Greenhouse Gas Emissions," North Carolina State University, 2008.

[10] R. Morshed, "Unnecessary Idling of Vehicles : An analysis of the current situation and what can be done to reduce it.," McMaster University, 2010.

[11] E. E. Lust, "SYSTEM-LEVEL ANALYSIS AND COMPARISON OF LONG-HAUL TRUCK IDLE-REDUCTION TECHNOLOGIES," University of Maryland, College Park, 2008.

[12] V. O'Grady, J. Tian, W. J. Seo, and J. H. Shim, "INVESTIGATING THE COST, LIABILITY AND RELIABILITY OF ANTI-IDLING EQUIPMENT FOR TRUCKS," 2007.

[13] E. E. Lust, W. T. Horton, R. Radermacher, G. L. M. Hall, and C. Park, "A REVIEW AND COST COMPARISON OF CURRENT IDLE-REDUCTION TECHNOLOGY," in *ASME Power 2008*, 2014, pp. 1–12.

[14] C. MacDonald, R. Douglas, A. Tamayol, and M. Bahrami, "A Feasibility Study of Auxiliary HVAC Systems for Reducing Idling Time of Long Haul Trucks," in *ASME 2012 Summer Heat Transfer*, 2012, pp. 323–330.

[15] F. Stodolsky, L. Gaines, and A. Vyas, "Analysis of Technology Options to Reduce the Fuel Consumption of Idling Trucks," Argonne, Jun. 2000.

[16] R. & A. E. C. LTD, "Truck stop electrification and anti-idling as a diesel emissions reduction strategy at U.S. -Mexico ports of Entery," 2009.

[17] Enowenergy Co., “Reducing Fleet Operating Costs Using Solar Powered Idle Reduction Technology,” 2014.

[18] B. Zalba, J. M. Marín, L. F. Cabeza, and H. Mehling, “Review on thermal energy storage with phase change: materials, heat transfer analysis and applications,” *Appl. Therm. Eng.*, vol. 23, no. 3, pp. 251–283, Feb. 2003.

[19] A. Sharma, V. V. Tyagi, C. R. Chen, and D. Buddhi, “Review on thermal energy storage with phase change materials and applications,” *Renew. Sustain. Energy Rev.*, vol. 13, no. 2, pp. 318–345, Feb. 2009.

[20] P. Wang, B. Song, Y. Wang, and L. Zhang, “Application of Concurrent Subspace Design to Shape Design of Autonomous Underwater Vehicle,” in *Eighth ACIS International Conference on Software Engineering, Artificial Intelligence, Networking, and Parallel/Distributed Computing (SNPD 2007)*, 2007, pp. 1068–1071.

[21] R. D. Braun, R. W. Powell, R. A. Lepsch, and D. O. Stanley, “Comparison of Two Multidisciplinary Optimization Strategies for Launch-Vehicle Design,” *J. Spacecr. Rockets*, vol. 32, no. 3, pp. 404–410, 1995.

[22] J. S.- Sobieski, “Multidisciplinary aerospace design optimization : survey of recent developments,” *Struct. Optim.*, vol. 14, no. 1, pp. 1–23, 1997.

[23] Y. He and J. McPhee, “Multidisciplinary design optimization of mechatronic vehicles with active suspensions,” *J. Sound Vib.*, vol. 283, no. 1–2, pp. 217–241, May 2005.

[24] Y. He and J. McPhee, “A design methodology for mechatronic vehicles: application of multidisciplinary optimization, multibody dynamics and genetic algorithms,” *Veh. Syst. Dyn.*, vol. 43, no. 10, pp. 697–733, Oct. 2005.

[25] Y. He and J. Mcphee, “Multidisciplinary Optimization of Multibody Systems with Application to the Design of Rail Vehicles,” *Multibody Syst. Dyn.*, vol. 14, no. 2, pp. 111–135, Sep. 2005.

[26] H. P. Computing and S. K. and J. S. Eszczanski-Sobieski, “Multidisciplinary design optimization — some formal methods , framework requirements , and application to vehicle design,” *Int. J. Veh. Des.*, vol. 25, no. 1, pp. 3–22, 2001.

[27] S. Kodiyalam, R. J. Yang, L. Gu, and C.-H. Tho, “Multidisciplinary design optimization of a vehicle system in a scalable, high performance computing environment,” *Struct. Multidiscip. Optim.*, vol. 26, no. 3–4, pp. 256–263, Feb. 2004.

[28] T.-Y. Chen and C.-M. Yang, “Multidisciplinary design optimization of mechanisms,” *Adv. Eng. Softw.*, vol. 36, no. 5, pp. 301–311, May 2005.

[29] Y.-C. Choi, J.-W. Lee, and Y.-H. ByUn, “Optimal Supersonic Air-Launching Rocket Design Using Multidisciplinary System Optimization Approach,” *J. Korean Soc. Aeronaut. Sp. Sci.*, vol. 33, no. 12, pp. 26–32, Dec. 2005.

[30] W. Gao, S. Member, S. K. Porandla, and S. Member, “Design Optimization of a Parallel Hybrid Electric Powertrain,” in *IEEE Vehicle Power and Propulsion Conference*, 2005, pp. 530–535.

[31] "Argonne TTRDC - Modeling, Simulation & Software - PSAT." [Online]. Available: http://www.transportation.anl.gov/modeling_simulation/PSAT/index.html.

[32] "ADVISOR Documentation." [Online]. Available: http://adv-vehicle-sim.sourceforge.net/.

[33] B. Zhang, Z. Chen, C. Mi, and Y. L. Murphey, "Multi-objective parameter optimization of a series hybrid electric vehicle using evolutionary algorithms," in *IEEE Vehicle Power and Propulsion Conference*, 2009, pp. 921–925.

[34] L. Fang and S. Qin, "Concurrent Optimization for Parameters of Powertrain and Control System of Hybrid Electric Vehicle Based on Multi-Objective Genetic Algorithms," in *SICE-ICASE International Joint Conference*, 2006, pp. 2424–2429.

[35] X. Liu, Y. Wu, and J. Duan, "Optimal Sizing of a Series Hybrid Electric Vehicle Using a Hybrid Genetic Algorithm," in *IEEE International Conference on Automation and Logistics*, 2007, pp. 1125–1129.

[36] B. Fan, A. Khajepour, and M. Kazerani, "Design of an Anti-Idling System for Police Vehicles," in *ASME 2010 International Design Engineering Technical Conferences & Computers and Information in Engineering Conference IDETC/CIE*, 2010, pp. 297–305.

[37] B. S. Fan, "Multidisciplinary Optimization of Hybrid Electric Vehicles : Component Sizing and Power Management Logic," University Of Waterloo, 2011.

[38] B. Huang, X. Shi, and Y. Xu, "Parameter Optimization of Power Control Strategy for Series Hybrid Electric Vehicle," in *IEEE International Conference on Evolutionary Computation*, 2006, pp. 1989–1994.

[39] Z. Wang, B. Huang, Y. Xu, and W. Li, "Optimization of Series Hybrid Electric Vehicle Operational Parameters By Simulated Annealing Algorithm," in *IEEE International Conference on Control and Automation*, 2007, pp. 1536–1541.

[40] Kozmaksan, "Kozmaksan hydraulic pumps and power take-offs."

[41] Muncie Power Products, "CS & CD SERIES PTOs."

[42] B. S. M. Fan, "Modeling and Simulation of A Hybrid Electric Vehicle Using MATLAB/Simulink and ADAMS," University of Waterloo, 2007.

[43] G. Rizzoni, L. Guzzella, and B. M. Baumann, "Unified modeling of hybrid electric vehicle drivetrains," *IEEE/ASME Trans. Mechatronics*, vol. 4, no. 3, pp. 246–257, 1999.

[44] L. Guzzella and C. H. Onder, *Introduction to Modeling and Control of Internal Combustion Engine Systems*. Springer, 2009.

[45] L. Guzzella and A. Sciarretta, *Vehicle propulsion systems*. Springer, 2007.

[46] H. He, R. Xiong, H. Guo, and S. Li, "Comparison study on the battery models used for the energy management of batteries in electric vehicles," *Energy Convers. Manag.*, vol. 64, no. 0, pp. 113–121, 2012.

[47] O. Tremblay, L. A. Dessaint, and A. I. Dekkiche, “A Generic Battery Model for the Dynamic Simulation of Hybrid Electric Vehicles,” in *IEEE Vehicle Power and Propulsion Conference*, 2007, pp. 284–289.

[48] O. Tremblay and L. Dessaint, “Experimental Validation of a Battery Dynamic Model for EV Applications,” *World Electr. Veh.*, vol. 3, pp. 1–10, 2009.

[49] W. Scott, “Impact of High Fidelity Battery Models for Vehicle Applications,” University of Waterloo, 2015.

[50] M. Chen and G. A. Rincon Mora, “Accurate electrical battery model capable of predicting runtime and I-V performance,” *IEEE Trans. Energy Convers.*, vol. 21, no. 2, pp. 504–511, 2006.

[51] “U . S . Department of Energy Vehicle Technologies Program Battery Test Manual For Plug-In Hybrid Electric Vehicles,” The Idaho National Laboratory, 2008.

[52] Statistics Canada, “Time with the family,” *Statistics Canada*, 2007. [Online]. Available: http://www.statcan.gc.ca/daily-quotidien/070213/dq070213b-eng.htm.

[53] B. Price, E. Dietz, and J. Richardson, “Life cycle costs of electric and hybrid electric vehicle batteries and End-of-Life uses,” in *IEEE International Conference on Electro/Information Technology*, 2012, pp. 1–7.

[54] N. Risk, “Application of Life- Cycle Assessment to Nanoscale Technology : Lithium-ion Batteries for Electric Vehicles,” 2013.

[55] K. Aguirre, L. Eisenhardt, C. Lim, B. Nelson, A. Norring, P. Slowik, and N. Tu, “Lifecycle Analysis Comparison of a Battery Electric Vehicle and a Conventional Gasoline Vehicle,” 2012.

[56] N. Shidore, J. Kwon, and A. Vyas, “Trade-off between PHEV fuel efficiency and estimated battery cycle life with cost analysis,” in *IEEE Vehicle Power and Propulsion Conference*, 2009, no. 978, pp. 669–677.

[57] P. Wolfs, “An Economic Assessment of ‘ Second Use ’ Lithium- Ion Batteries for Grid Support,” in *Universities Power Engineering Conference (AUPEC)*, 2010.

[58] Mathworks, “Global Optimization Toolbox User ’ s Guide R 2014 a,” 2014.

[59] Mustang Advanced Engineering, “Mustang Dynamometer,” Twinsburg, 2012.

[60] “EPA Urban Dynamometer Driving Schedule (UDDS).” [Online]. Available: http://www.epa.gov/oms/standards/light-duty/udds.htm. [Accessed: 01-Mar-2015].

[61] Q. Gong, S. Midlam-Mohler, V. Marano, and G. Rizzoni, “An Iterative Markov Chain Approach for Generating Vehicle Driving Cycles,” *SAE Internatinal J. Engines*, vol. 4, no. 1, pp. 1035–1045, Apr. 2011.

[62] D. E. Goldberg, *Genetic Algorithms in Search , Optimization , and Machine Learning*. Addison-Wesley, 1953.

[63] D. E. Goldberg and J. H. Holland., “Genetic Algorithms and Machine Learning,” *Mach. Learn.*, vol. 3, no. 2, pp. 95–99, 1988.

[64] J. S. R. Jang and C. T. Sun, *Neuro-fuzzy and soft computing: a computational approach to learning and machine intelligence*. Prentice-Hall, Inc., 1996.

[65] J. H. Holland, *Adaptation in natural and artificial systems: An introductory analysis with applications to biology, control, and artificial intelligence.* U Michigan Press, 1975.

[66] V. Cerny, "Thermodynamical Approach to the Traveling Salesman Problem : An Efficient Simulation Algorithm," *J. Optim. Theory Appl.*, vol. 45, no. 1, pp. 41–51, 1985.

[67] S. Kirkpatrick, C. D. Gelatt, and M. P. Vecchi, "Optimization by simulated annealing.," *Science*, vol. 220, no. 4598, pp. 671–80, May 1983.

Appendix A
Optimization Methods

In this appendix, two common optimization techniques suitable for the optimization problem at hand are discussed below.

- **Genetic Algorithm (GA)**

The GA method [62]–[64] is an optimization method based on the concepts of natural selection and evolution processes. It has a variety of advantages for problems similar to this study: i) It can be used for both continuous and discrete problems, ii) it is a derivative-free optimization method which can be implemented for problems with very complex objective functions such as parameter identification and component sizing, iii) it is a random based search method, which tries to find the optimum result.

The Genetic Algorithm was first presented by John Holland at the University of Michigan in the early 1970s, and it was covered in his book "Adaptation in Natural and Artificial Systems" (1975) [65]. From that time, it has been widely used in different research works and programmed in different software.

In this study, the MATLAB software is used for the implementation of GA. Every software has generally the same process for solving GA problems. First, each of the variables is encoded into a binary string called a "Gene". In the next step, genes will combine with each other to create "Chromosomes". A non-negative real value is assigned to each chromosome called "Fitness". The goal of GA is to maximize the fitness; hence, in software such as MATLAB, fitness is defined such that maximizing the fitness value results in minimizing the desired objective function.

In the optimization process, the population of the chromosomes is randomly generated and then advanced repeatedly to a better overall fitness value. In each iteration, the algorithm produces a new population using operators such as “Crossover” and “Mutation”. The members (chromosomes or parents) with higher fitness values have more chance to take part in mating operations, but other parents, even with low fitness values, always have a little chance as well. This feature of the GA helps the operation to escape from the local optimum points and search for the optimal results [58].

In each generation, the fitness value of all chromosomes is calculated and then the selection operation determines which parents will take part in the mating pool in order to produce the next generation. The crossover operation will be applied after the parents are selected to create the next generation. The GA selects two parents randomly from the mating pool. Then, based on the “Crossover Rate” value, it is determined whether a crossover should take place or not. Usually, the Crossover Rate is more than 0.6.

After a crossover operation, the mutation happens. Selection and crossover operations create a number of different chromosomes. However, there is the possibility that there is not enough variety of chromosomes and whether or not GA had searched the entire problem space, mostly due to the initial parents chosen and the local optimums. Mutation makes small random changes in the chromosomes, which help the GA to search a broader space. In this operation, with a low probability called the “Mutation Rate”, flipping a bit in the binary string (from 0 to 1 or 1 to 0) is applied to the selected chromosome. Usually, the mutation rate is less than 0.5. As the mutation rate increases, the GA will approach a simple random search.

The GA process will be repeated until a terminating criterion is satisfied. There are a variety of criteria in MATLAB. In this work, the optimization is terminated because the average change in the fitness value was less than 50, which reperesents the total system cost tolerance of 50 dollars.

- **Simulated Annealing (SA)**

Simulated annealing is an optimization method which named based on the annealing process in metallurgy, where the concept is to control the heat for the slow cooling of materials to ensure a suitable solidification of crystal while reducing defects. This technique ensures a crystalline state related to the lowest energy. This method was first proposed by 2 groups of researchers namely: Scott Kirkpatrick, C. Daniel Gelatt, Mario P. Vecchi, and Vlado Černý in the 1980s [66], [67].

The optimization problem is defined to minimize the objective function $J(X)$, where X is a vector of the optimization variables. Vector X is limited among its upper and lower bounds. The algorithm needs a starting point (X_1) and then randomly moves along each coordinate direction to reach a new point with a better objective function value. In each iteration, if the value of the objective function in the new point gets better (the value decreases), the new point is accepted and considred as the initial point for the next iteration. If there is no modifiation in the value of the new point, the new point is accepted with a probability of:

$$P = e^{\frac{-\Delta J}{K_{SA} T_{SA}}} \tag{A-1}$$

in which ΔJ is the difference between the old and new point, K_{SA} is Boltzmann's constant scaling factor, and T_{SA} is the material temperature. The initial temperature (T_{SA0}) is "high", like the first condition of the material during metallurgy. A series of posible solutions is genarated till the average value of J stabilizes as K_{SA} increases, this condition is considered as an equilibrium. When the

optimization reaches a thermal equilibrium, temperature T_{SA} is reduced and a new series of solutions is genarated until the thermal equilibrium is reached in the new temperature $T_{SA.}$ This operation will continue until an acceptable low temperature accrues and the optimal minimum is found.

The benefit of the SA method is that the choosing of the initial starting point (X_1) will not affect the final solution value; however, it will affect the optimization time remarkably. SA could also be used for both continous or discrete problems and differentiate free problems.